A&A 672, A183 (2023)
https://doi.org/10.1051/0004-6361/202245713

Astronomy & Astrophysics

Astrophysical properties of 15062 *Gaia* DR3 gravity-mode pulsators

Pulsation amplitudes, rotation, and spectral line broadening⋆

C. Aerts[1,2,3,4], G. Molenberghs[5,6], and J. De Ridder[1]

[1] Institute of Astronomy, KU Leuven, Celestijnenlaan 200D, 3001 Leuven, Belgium
e-mail: conny.aerts@kuleuven.be
[2] Department of Astrophysics, IMAPP, Radboud University Nijmegen, PO Box 9010, 6500 GL, Nijmegen, The Netherlands
[3] Max Planck Institute for Astronomy, Koenigstuhl 17, 69117 Heidelberg, Germany
[4] Guest Researcher, Center for Computational Astrophysics, Flatiron Institute, 162 Fifth Ave, New York, NY 10010, USA
[5] I-BioStat, Universiteit Hasselt, Martelarenlaan 42, 3500 Hasselt, Belgium
[6] I-BioStat, KU Leuven, Kapucijnenvoer 35, 3000 Leuven, Belgium

Received 17 December 2022 / Accepted 8 February 2023

ABSTRACT

Context. Gravito-inertial asteroseismology came into existence thanks to high-precision CoRoT and *Kepler* space photometric light curves. So far, it has given rise to the internal rotation frequency of a few hundred intermediate-mass stars, yet only several tens of these have been weighed, sized, and age-dated with high precision using asteroseismic modelling.
Aims. We aim to increase the sample of optimal targets for future gravito-inertial asteroseismology by assessing the properties of 15062 newly found *Gaia* DR3 gravity-mode pulsators. We also wish to investigate whether or not there is a connection between their fundamental parameters, the dominant mode, and their spectral line broadening as measured by *Gaia*.
Methods. After reclassifying about 22% of the F-type gravity-mode pulsators as B-type according to their effective temperature, we constructed histograms of the fundamental parameters and mode properties of the 15062 new *Gaia* DR3 pulsators. We compared these histograms with those of 63 *Kepler* bona fide class members. We fit errors-in-variables regression models to couple the effective temperature, luminosity, gravity, and oscillation properties to the two *Gaia* DR3 parameters capturing spectral line broadening for a fraction of the pulsators.
Results. We find that the selected 15062 gravity-mode pulsators have properties that are fully in line with those of their well-known *Kepler* analogues, revealing that *Gaia* has a role to play in asteroseismology. The dominant g-mode frequency is a significant predictor of the spectral line broadening for the class members for which this quantity has been measured. We show that the *Gaia* `vbroad` parameter captures the joint effect of time-independent intrinsic and rotational line broadening and time-dependent tangential pulsational broadening.
Conclusions. While the *Gaia* mission was not designed to detect non-radial oscillation modes, its multitude of data and homogeneous data treatment allow us to identify a vast number of new gravity-mode pulsators that have fundamental parameters and dominant mode properties in agreement with those of such *Kepler* bona fide pulsators. This large new sample of *Gaia* DR3 pulsators can be followed up with dedicated high-precision photometric or high-resolution spectroscopic instruments to embark on asteroseismic modelling.

Key words. asteroseismology – methods: statistical – astronomical databases: miscellaneous – stars: oscillations – stars: rotation – stars: interiors

1. Introduction

The *Gaia* space mission of the European Space Agency (Gaia Collaboration 2016b) is currently revolutionising the entire field of astrophysics. Although *Gaia* is first and foremost an astrometric mission, it also delivers the largest homogeneous survey of broad-band photometric and medium-resolution spectroscopic data achieved to date (Gaia Collaboration 2016a). While the *Gaia* mission was not designed to deliver input for the research field of asteroseismology (Aerts et al. 2010), it does contribute important information for this recent emerging topic within stellar astrophysics. Indeed, aside from stellar luminosities deduced from the high-precision parallaxes (Bailer-Jones et al. 2018), the *Gaia* instrumentation also delivers years-long photometric time-series data at millimagnitude (mmag) precision in the *Gaia* G-band. Although these *Gaia* G light curves are only sparsely sampled, they do allow us to populate a wide range of stellar variability classes (see Eyer & Mowlavi 2008, for a description of the 'variability tree'). In particular, the *Gaia* DR3 time-series data allow us to revisit studies of the classes of pulsating variables (cf., Aerts et al. 2010, Chapter 2) with many more class members each. Rimoldini et al. (2023) classified more than 12 million variables, among which there are RR Lyr stars (Clementini et al. 2023), Cepheids (Ripepi et al. 2023), young stellar objects (Marton et al. 2023), and long-period variables (Lebzelter et al. 2023).

⋆ Data files with the *Gaia* identification, fundamental parameters, dominant frequency and its amplitude, and the line broadening values for all 15062 stars in the studied sample are only available at the CDS via anonymous ftp to `cdsarc.cds.unistra.fr` (`130.79.128.5`) or via `https://cdsarc.cds.unistra.fr/viz-bin/cat/J/A+A/672/A183`

In the present work, we focus on stars observed by *Gaia* and classified from its Data Release 3 (DR3; Gaia Collaboration 2021, 2023b) as gravity-mode (g-mode hereafter) pulsators by Coordination Unit 7, which treated variable stars (Holl et al. 2018; Gaia Collaboration 2019; Eyer et al. 2023). In their *Gaia* DR3 Performance Verification Paper (PVP), Gaia Collaboration (2023a, hereafter Paper I) assigned the stars we revisit in the present study to the classes of the slowly pulsating B stars (SPB stars; Waelkens 1991; De Cat & Aerts 2002) or γ Doradus stars (γ Dor stars; Kaye et al. 1999; Handler 1999). These main sequence g-mode pulsators are the best laboratories for asteroseismic probing of the deep interior of dwarfs with a mass of between 1.3 $M_\odot$ and 9 $M_\odot$ (Aerts 2021, for a general review of the asteroseismology of such stars). There are now hundreds of single and binary dwarfs with a convective core for which the rotation has been measured just outside the core from a series of consecutive radial-order dipole g-mode oscillations (Kurtz et al. 2014; Triana et al. 2015; Keen et al. 2015; Saio et al. 2015; Van Reeth et al. 2016, 2018; Moravveji et al. 2016; Murphy et al. 2016; Pápics et al. 2017; Zwintz et al. 2017; Li et al. 2019, 2020; Sekaran et al. 2021). Both the γ Dor and SPB pulsators reveal time-dependent spectral-line variations due to the tangential velocity fields at the stellar surface (Aerts et al. 1999, 2004; De Cat & Aerts 2002; De Cat et al. 2006). These pulsators are intermediate-mass dwarfs in the core hydrogen-burning phase without strong stellar winds.

The *Gaia* DR3 light curves analysed in Paper I resulted in an order-of-magnitude increase in the population of the two classes of non-radial g-mode main sequence pulsators. The positions of these new candidate SPB and γ Dor pulsators in the Hertzsprung-Russell (HR) diagram were compared with theoretically predicted instability strips, each of which is based on the dominant excitation mechanism for one particular choice of input physics, leading to coherent g-modes with infinite lifetime in Paper I. It was found that many of the *Gaia* g-mode pulsators occur outside the borders of such instability strips for these two classes of g-mode pulsators. This was ascribed to inaccuracies in the *Gaia* effective temperature, their fast rotation, and/or different input physics or (past) binarity not treated in instability predictions, in addition to too low values for the opacities of heavy elements such as iron and nickel in the excitation layers, as is well known from previous excitation studies of SPB pulsators (Moravveji 2016; Daszyńska-Daszkiewicz et al. 2017; Szewczuk & Daszyńska-Daszkiewicz 2017). Moreover, aside from coherent eigenmodes with long lifetime driven by opacity layers or those at the bottom of the outer convective envelope, internal gravity waves with short lifetimes – which are excited at the interface between the convective core and/or the convective outer envelope and radiative zones – have been suggested from multi-dimensional hydrodynamical simulations mimicking dwarfs in the considered mass regime (Rogers et al. 2013; Grassitelli et al. 2015a,b; Edelmann et al. 2019; Horst et al. 2020). All these predicted g-modes and internal gravity waves act together in the stellar interior and those reaching the stellar surface with detectable amplitude give rise to complex light curves and time-dependent variations of the spectral line profile. This is in agreement with large, modern, time-resolved space photometric surveys delivering μmag precision and highlighting a continuous coverage of observed intermediate-mass pulsating dwarfs along the main sequence (Uytterhoeven et al. 2011; Bowman et al. 2019, 2020; Pedersen et al. 2019; Antoci et al. 2019; Balona & Ozuyar 2020, and Paper I) that followed the earlier, similar findings from the high-resolution ground-based time-resolved spectroscopy mentioned above.

Here, we study the astrophysical properties of the new *Gaia* DR3 g-mode pulsators found in Paper I. We consider all the pulsators for which the luminosity, effective temperature, and gravity have been determined by the *Gaia* Data Processing Analysis Consortium (DPAC; Gaia Collaboration 2016a, 2021). We compare the properties of these *Gaia* DR3 g-mode pulsators with those of our sample of 63 of the best-known bona fide g-mode pulsators observed with the NASA *Kepler* space telescope, for which high-resolution follow-up spectroscopy was assembled and interpreted. These *Kepler* and spectroscopic data led to the identification of dipole g-modes of consecutive radial order and to asteroseismic modelling for these 63 dwarfs (Mombarg et al. 2021; Pedersen et al. 2021).

In the current follow-up study of Paper I, we consider the amplitude of the dominant frequency in the *Gaia* G-band and relate it to the fundamental parameters for both the *Gaia* DR3 and *Kepler* g-mode pulsators. Moreover, we consider the subsamples of *Gaia* DR3 g-mode pulsators for which an estimation of the spectral line broadening is available from *Gaia*'s Radial Velocity Spectrometer (RVS) within the large homogeneous *Gaia* DR3 data set (Creevey et al. 2023; Frémat et al. 2023). Our general aim is to search for relationships between the fundamental parameters and pulsational properties of g-mode pulsators. In particular, we investigate if there is any connection between the properties of the dominant g-mode of the stars and their rotation and/or spectral line broadening. So far, similar studies have been hampered by small sample sizes (Aerts et al. 2014a) or by separate and/or inhomogeneous treatment of statistical modelling based on the observables deduced from photometric and spectroscopic data (Simón-Díaz et al. 2017; Burssens et al. 2020). Although the *Gaia* photometric and spectroscopic instruments were not designed to study non-radial oscillations, nor were they optimised to deduce the line broadening of stars hotter than 7000 K, DR3 does provide unprecedentedly large samples of homogeneously treated g-mode pulsators in terms of their line broadening and fundamental parameters.

We discuss the sample selection for the current paper in Sect. 2 and consider the fundamental parameters and dominant variability characteristics of 15062 g-mode pulsators in Sect. 3 and Sect. 4, respectively. Section 5 focuses on the astrophysical interpretation of the measured spectral line broadening of the sample, which is based on the method of errors-in-variables and on multi-variable regression models constructed using the 'backward selection' technique. We discuss our findings and conclude in Sect. 6.

2. Sample selection

Paper I resulted in 106 207 *Gaia* DR3 main sequence pulsators of spectral types O, B, A, or F fullfilling four criteria: (1) their *Gaia* DR3 G light curve consists of at least 40 epochs; (2) their dominant cyclic frequency (denoted here as ν) in the *Gaia* G light curve occurs in the range $[0.7, 25]$ day^{-1}; (3) this frequency ν differs from any of the instrumental frequencies 4, 8, 12, 16, 20, and 24 day^{-1} by more than 0.05 day^{-1}; and (4) ν has a false-alarm probability (FAP) according to the definition by Baluev (2008) of below 0.001. Despite these already strict selection criteria, additional restrictions on the frequency interval to which ν must belong for each of the four considered pulsation classes were imposed in Paper I to beat instrumental effects in Fourier space, because they occur at mmag level and intervene with the signal of non-radial oscillations also occurring at such a level for dwarf stars of intermediate mass.

The following four classes of pulsators were considered in Paper I: β Cep stars, SPB stars, δ Sct stars, and γ Dor stars (cf. Aerts et al. 2010, Chapter 2). We refer to Paper I and its literature references for details of the additional selection rules imposed upon ν based on common knowledge of the pulsational properties of these four well-known classes of variables, but reiterate here that the dominant modes of β Cep and δ Sct stars are p-modes with observed frequencies typically above 3 day^{-1}, while SPB and γ Dor stars have dominant g-modes with observed frequencies mostly below 3 day^{-1}, except for the fastest rotators.

Within the sample of 106 207 candidate pulsators assigned to the four pulsation classes in Paper I, those with frequencies above the spin frequency of the *Gaia* satellite are most affected by mmag-level instrumental effects, which may lead to spurious frequencies unrelated to the star. For this reason, we focus here on the two classes of main sequence pulsators, which have a dominant frequency well below the 4 day^{-1} spin frequency of the *Gaia* satellite. For now, with the relatively sparse DR3 light curves, this is the best approach to study the astrophysical properties of the *Gaia* DR3 g-mode pulsators without being contaminated by spurious instrumental frequencies.

The Appendix B of Paper I discussed the results for the dominant frequency ν in the *Gaia* DR3 light curves of the 63 bona fide g-mode pulsators (26 SPB and 37 γ Dor stars) whose entire amplitude spectrum is known with a level of precision of better than about 10^{-6} day^{-1} in cyclic frequency and a few μmag in amplitude (Van Reeth et al. 2015; Pedersen et al. 2021). Aerts et al. (2021) relied on the mode identification for all these stars' detected and identified dipole modes of consecutive radial order in order to deduce the convective and wave Rossby numbers for these best-known *Kepler* g-mode pulsators, covering the mass range from 1.3 $M_\odot$ up to about 9 $M_\odot$. All 63 pulsators have a dominant *Gaia* G amplitude, A_ν, of below 35 mmag and their dominant frequency occurs in the interval $\nu \in [0.7, 3.2]$ day^{-1} (see Figs. B.1 and B.2 in Paper I). Some of the new g-mode pulsators identified from *Gaia* DR3 in Paper I have higher dominant frequencies. Moreover, some of the *Gaia* DR3 g-mode pulsators have frequencies that are hard to unravel from the *Gaia* instrument frequencies caused by the spinning of the satellite.

Guided by Figs. B.1 and B.2 in Paper I, which summarise the dominant frequency and amplitude for the 63 bona fide *Kepler* g-mode pulsators, we further apply a fifth and sixth constraint in this work in addition to the selecton criteria of Paper I mentioned above; namely we demand that (5) $\nu \in [0.7, 3.2]$ day^{-1} and (6) $A_\nu \leq 35$ mmag. These two extra restrictions are applied to the SPB and γ Dor stars assigned to those two g-mode pulsator classes in Paper I. This is to ensure that we are dealing with non-radial oscillations rather than satellite frequencies. Moreover, we restrict these two samples to those pulsators for which a measurement of log L, log $T_{\rm eff}$, and log g is found in the DR3 `gspphot` tables. We use those values in order to maximise the sample size of g-mode pulsators treated in one homogeneous way by DPAC routines, given that we need to cover temperatures from ∼6 500 K all the way up to 25 000 K (see Paper I for details and Gaia Collaboration 2023b; Creevey et al. 2023).

A continuous coverage of pulsating B, A, and F stars along the main sequence is found in Paper I, in agreement with *Kepler* and TESS results (e.g. Balona & Ozuyar 2020). As the variability classification used in Paper I relied only on the *Gaia* G-band DR3 light curves, it cannot distinguish between B- and F-type pulsators without spectroscopic information (cf., Pedersen et al. 2019; Gebruers et al. 2021). On the other hand, the *Kepler* data clearly reveal that γ Dor and SPB pulsators have different astrophysical and pulsational properties (Van Reeth et al. 2015; Saio et al. 2018; Pedersen et al. 2021). We therefore wish to treat them as two separate classes, and we do so by relying on the *Gaia* DR3 effective temperature to reclassify the g-mode pulsators. Following the upper limit in effective temperature from the instability predictions by Xiong et al. (2016) for γ Dor stars, we use $T_{\rm eff} = 8500$ K to distinguish between γ Dor and SPB candidates. In practice, we reclassify all γ Dor candidates as SPB stars if their effective temperature is above 8500 K and, vice versa, we re-assign all SPB stars with a temperature of below 8500 K as γ Dor pulsators. This leads to a reclassification of 3244 γ Dor candidates as new SPB pulsators based on their *Gaia* DR3 effective temperature. This reassignment gives a fractional membership of 29% SPB and 71% γ Dor pulsators, which is fully in line with a Salpeter-type initial mass function (IMF; Salpeter 1955) for the typical masses of 1.6 $M_\odot$ for γ Dor stars (Mombarg et al. 2021) and of 4 $M_\odot$ for SPB stars (Pedersen 2022a). As we discuss below, another choice of the threshold temperature with which to distinguish the two classes does not impact our results.

A critical aspect of the current study compared to other surveys of g-mode pulsating dwarfs is that all the DR3 data and observables were obtained in one homogeneous way in terms of data selection and analysis. This is in contrast to the treatment of ground-based photometry and spectroscopy obtained for the much smaller dedicated asteroseismology samples for these two classes so far. While *Gaia* DR3 can only deliver the dominant mode at this stage, it provides by far the largest homogeneous survey of γ Dor and SPB pulsators to date.

3. Fundamental parameters of the g-mode pulsators in the two samples

Figures 1–3 show the histograms of the effective temperature, surface gravity, and luminosity for all 15 062 *Gaia* DR3 g-mode pulsators in our two samples taken from the `gspphot` tables, in comparison with those quantities deduced for the 63 bona fide pulsators. For the latter, we took the high-precision values for these quantities from detailed asteroseismic modelling of their interior based on numerous identified dipole g-modes by Pedersen (2022a, 26 SPB stars) and Mombarg et al. (2021, 37 γ Dor stars). Both these latter asteroseismic studies followed the methodology in Aerts et al. (2018) for the modelling of the internal structure of these stars. In order to be able to compare the distributions of the samples with vastly different numbers of stars, we show the normalised histograms as percentages of the entire sample population. For the γ Dor stars, the distributions of the effective temperature ($T_{\rm eff}$) and luminosity (log($L/\mathcal{L}_\odot$), with $\mathcal{L}_\odot$ being the solar luminosity) agree remarkably well between the 37 bona fide pulsators and the 11636 *Gaia* DR3 pulsators, revealing *Gaia*'s power to deduce these two fundamental parameters for large samples of such hot F-type pulsators. The gravities are somewhat lower than the asteroseismic values. Comparing the *Gaia* radii deduced from the DR3 $T_{\rm eff}$ and log $(L/\mathcal{L}_\odot)$ values shown in the left panel of Fig. 4 reveals that they are entirely compatible with the asteroseismic distribution, keeping in mind that the latter only consists of 37 pulsators.

As for the SPB stars, the *Gaia* DR3 sample is concentrated in the lower part of the SPB instability strip, as already found in Paper I. This latter paper also reported some possible systematic biases in the astrophysical parameters of hot stars as derived from the *Gaia* DR3 `gspphot` tables; more specifically, shifts to lower temperatures due to poorly estimated reddening. As we only work with the dominant frequency, we cannot exclude

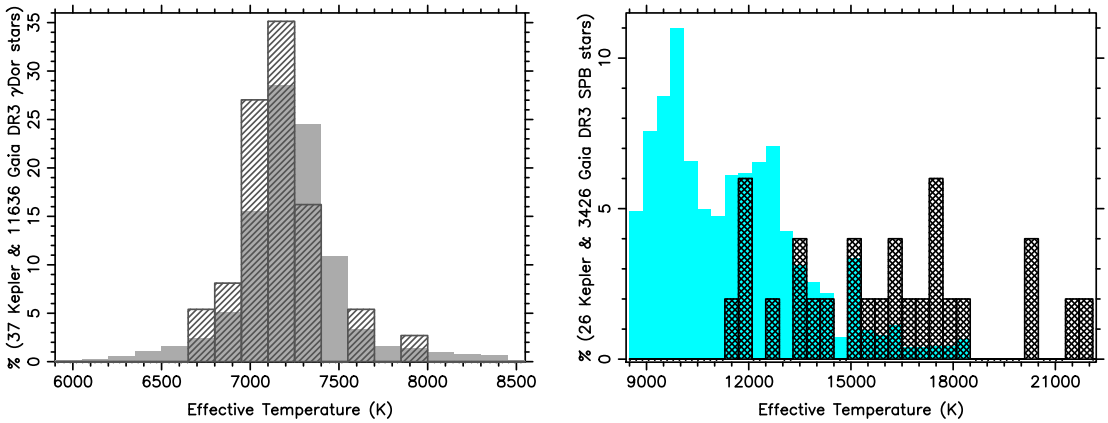

Fig. 1. Histograms (normalised to 100% occurrence) of the `gspphot` values for $T_{\rm eff}$ for 11 636 *Gaia* DR3 γ Dor stars (left, grey) and 3426 SPB stars (right, cyan). The width of the bars is in accordance with the average error (150 K for γ Dor and 400 K for the SPB stars). Asteroseismic values obtained from *Kepler* data are shown for 37 γ Dor (grey, hatched) and 26 SPB stars (black cross-hatched), respectively. For the right panel, 31 SPB stars with a temperature above 22 000 K in the *Gaia* DR3 sample were omitted for visibility reasons.

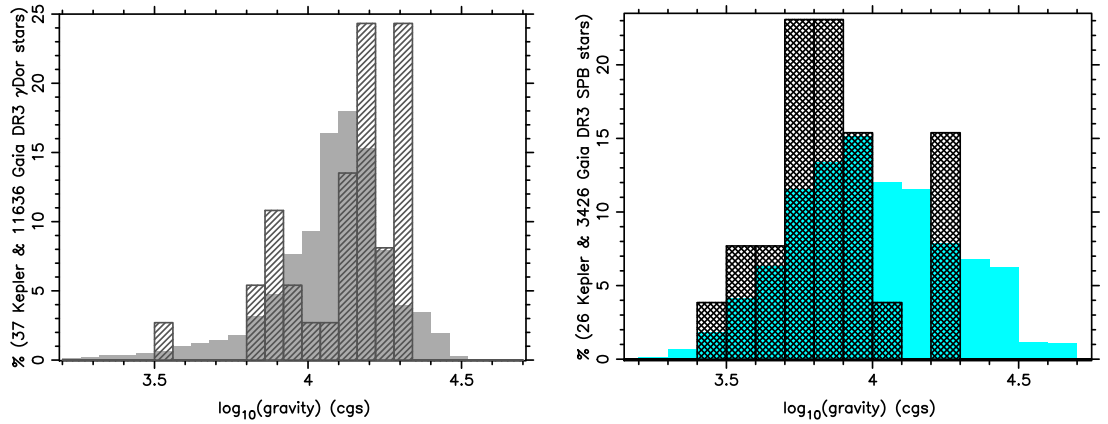

Fig. 2. Same as Fig. 1 but for log g.

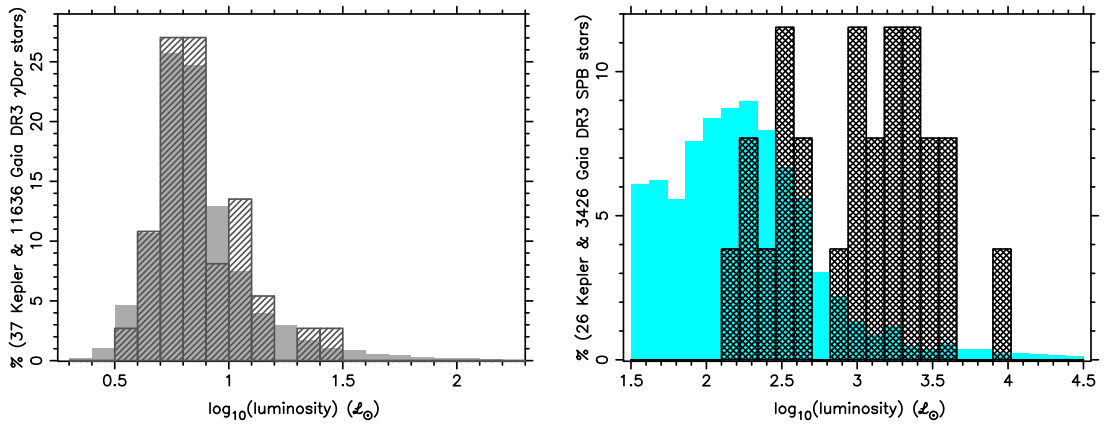

Fig. 3. Same as Fig. 1 but for log $(L/\mathcal{L}_\odot)$.

that some of the (reclassified) cool SPB stars are actually early A-type stars with rotational modulation. The majority of the 3426 SPB stars in our sample have relatively low *Gaia* luminosities compared to the 26 SPB stars in the asteroseismic sample. These two aspects combined limit the power of *Gaia* DR3 to estimate radii based on the `gspphot` tables for the entire class of SPB stars, yet the radius distribution of the 3426 SPB stars is compatible with that of the 26 bona fide SPB stars (Fig. 4, right panel).

Overall, the distributions for the three fundamental parameters $T_{\rm eff}$, log g, and log $(L/\mathcal{L}_\odot)$ of the *Gaia* γ Dor and SPB stars are in good agreement with the asteroseismic values of the bona fide *Kepler* pulsators in these two classes, keeping in mind that the *Gaia* sample of SPB stars mainly contains cool class members. We conclude that *Gaia* DR3 `gspphot` values lead to distributions for the radii as expected for g-mode pulsators when compared with the asteroseismic radii of the 63 bona fide pulsators.

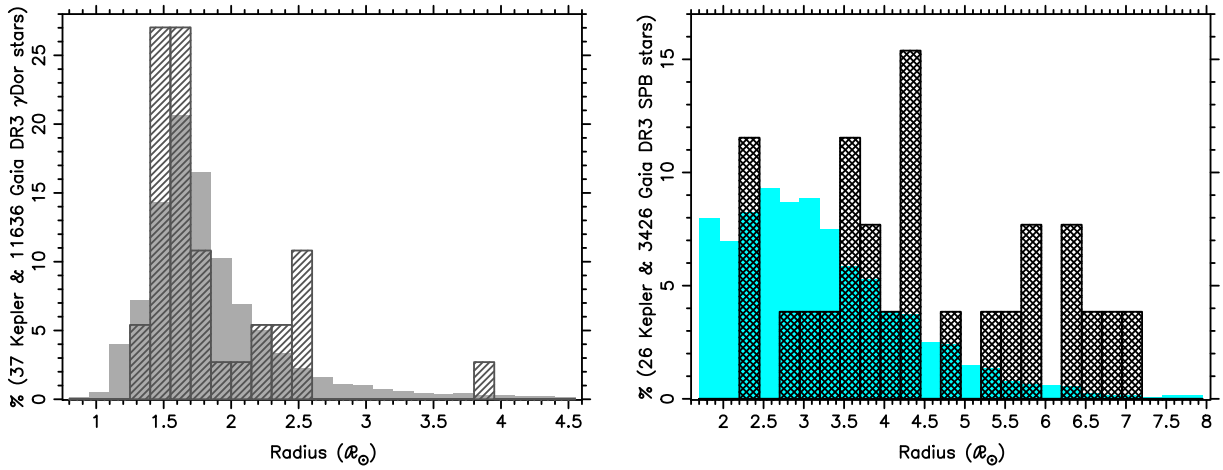

Fig. 4. Same as Fig. 1 but for the radius of the stars deduced from $\log(L/\mathcal{L}_\odot)$ and $T_{\rm eff}$.

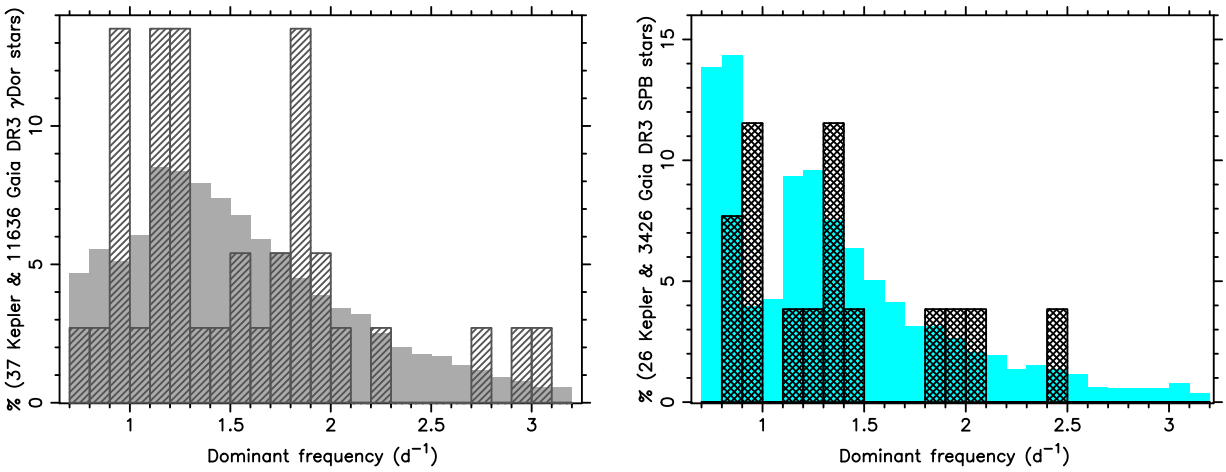

Fig. 5. Same as Fig. 1 but for the dominant frequency in the *Gaia G* light curve.

4. Pulsational properties of the dominant *g*-modes

As already emphasised in Paper I, *Gaia* has a good capacity to detect non-radial oscillation modes in main sequence stars. The two *Gaia g*-mode pulsator samples treated here result from relatively strict selection rules on the *Gaia G* photometric light curves, yet they are already an order of magnitude larger than the corresponding *Kepler* samples. Despite the sparse *Gaia* sampling, it is to be anticipated that many more *g*-mode pulsators will be selected when the DR4 and DR5 data sets become available.

Figure 5 shows the distributions for the dominant frequency in the DR3 *Gaia G*-band light curves. Overplotted are the distributions for the dominant frequency deduced from the four-year, uninterrupted high-cadence *Kepler* light curves of far better precision taken from Van Reeth et al. (2015) and Pedersen et al. (2021) for the γ Dor and SPB stars, respectively. We recall that we used the dominant *g*-mode frequency range covered by these two samples of bona fide *g*-mode pulsators as a selection criterion to restrict the *Gaia* DR3 samples to pulsators adhering to this same appropriate frequency range. It is therefore built in that we find compatible ranges. Nevertheless, the distributions of the *Gaia* DR3 and *Kepler* pulsators are also in reasonably good agreement, keeping in mind the small samples sizes for the latter.

Figure 6 shows histograms for the amplitude of the dominant frequency found in the *Gaia G* light curve. These bona fide pulsators did not survive our six selection criteria, mainly because they have fewer than 40 epochs in *Gaia* DR3 and/or their dominant frequency did not meet the FAP criterion. In order to be able to compare the amplitudes between the *Gaia* DR3 and *Kepler* pulsators, and to exclude instrumental effects for the bona fide pulsators, we computed their *Gaia G* amplitude from a best-fit regression model obtained by imposing the dominant frequency found in their *Kepler* light curve onto the *Gaia G* data, irrespective of the number of epochs in the latter or the frequency's FAP value. Both histograms in Fig. 6 visualise the current detection threshold to find *g*-modes in the *Gaia G* light curves. It is seen that DR3 allows us to detect *g*-mode frequencies with an amplitude of above 4 mmag. The *Kepler* data delivered *g*-modes with far lower amplitudes as seen in the histogram, because the mission was designed to assemble μmag-precision uninterrupted photometry with 30 min cadence for exoplanet hunting (Borucki et al. 2010) and for asteroseismology (Gilliland et al. 2010). We find that the *g*-mode amplitude distributions deduced from *Gaia* DR3 and *Kepler* data only barely overlap for the class of

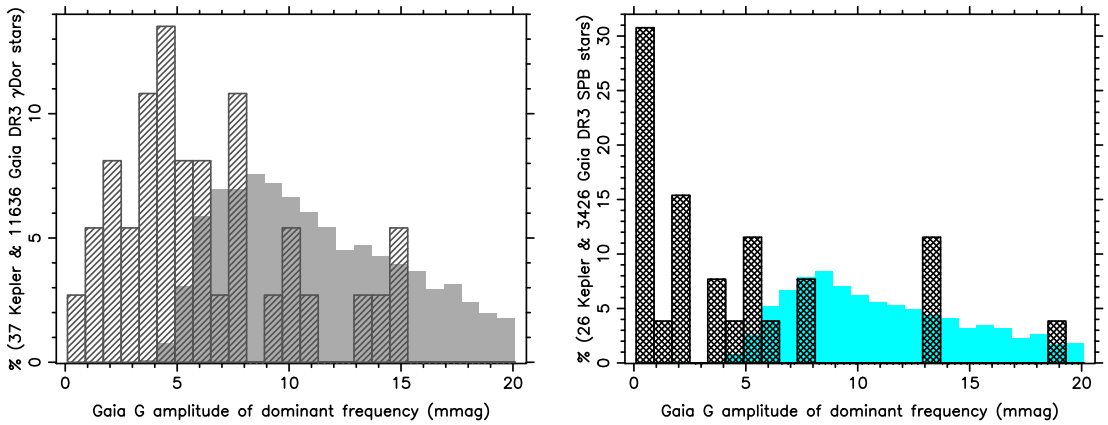

Fig. 6. Same as Fig. 1 but for the amplitude of the dominant frequency in the *Gaia G* light curve. For the bona fide γ Dor and SPB pulsators, we computed the amplitude by fitting a harmonic signal to the *Gaia* time series using the main frequency derived from the four-year *Kepler* light curve.

the SPB pulsators, as most of the 26 bona fide *Kepler* SPB stars have low dominant amplitudes outside *Gaia*'s reach.

5. Properties of spectral line broadening

Aside from photometric and astrometric data, the *Gaia* satellite also delivers spectroscopic data. Its spectrometer RVS has a median resolving power of 11 500 and is sensitive to the wavelength range from 846 to 870 nm. While it was primarily designed to measure the radial velocity of as many *Gaia* sources as possible (Katz et al. 2023), we use the RVS data to study the spectral line broadening of g-mode pulsators. Our aim is to investigate whether or not there is any connection between the overall line broadening, the fundamental parameters, and the oscillation properties for the two large *Gaia* DR3 samples of g-mode pulsators, as suggested previously based on line-profile simulations (Aerts et al. 2009; Aerts & Rogers 2015). While RVS on average provides a resolving power of only $\sim$26 km s^{-1}, non-radial oscillations generate variations in the width and the skewness of spectral lines (Aerts & De Cat 2003) and these may affect the way that the line broadening values are determined (we refer to Frémat et al. 2023, for a detailed description).

Line-profile variations caused by the g-modes of γ Dor and SPB stars occur at the level of several to tens of km s^{-1} in the centroid of the line (e.g. Aerts et al. 1999; De Cat et al. 2000, 2006; Mathias et al. 2001, 2004; De Cat & Aerts 2002). High-resolution time-series spectroscopy of bright g-mode pulsators is a powerful tool to identify the spherical wavenumbers (l, m) of the dominant oscillation mode(s) provided that the oscillation cycle is well covered (Briquet et al. 2003; De Cat et al. 2005). Such applications couple the velocity field – which is computed from the theory of non-radial oscillations – to the observed line-profile variations in order to infer the radial and tangential components of the velocity vector due to each non-radial oscillation mode (Aerts et al. 2010, Chapter 6). This requires that the spectroscopy has high resolving power and signal-to-noise ratio (S/N), typically above 50 000 and 300, respectively (Aerts & De Cat 2003).

In the absence of high-quality spectroscopy, or in the case where only a few snapshot spectra are available, line-profile modelling by means of the proper time-dependent pulsational velocity field is impossible. In such a case, it is customary to approximate the overall line broadening due to oscillations and rotation together using a single time-independent function called macroturbulence (Simón-Díaz et al. 2010). Although its functional form assumes a symmetrical line profile (cf. Aerts et al. 2014b, Fig. 9), the macroturbulence correlates strongly with quantities representing the line-profile variability (Simón-Díaz et al. 2017), such as the velocity moments (Balona 1986; Aerts et al. 1992).

Fitting time-resolved line-profile variations due to oscillations or spots artificially with a symmetrical macroturbulent profile leads to time variability in the macroturbulence, which is in excellent agreement with the mode frequencies or rotation periods of intermediate-mass dwarfs (Aerts et al. 2014b). This suggests that macroturbulence is merely a downgraded (and often poor) time-independent symmetrical simplification of the true spectral line profiles caused by oscillations and/or spots. Nevertheless, in the absence of time-resolved spectroscopy, it is a sensible approach to fit the line profiles of snapshot spectra with a synthetic time-independent macroturbulent broadening profile, particularly for large surveys of stars such as those offered by *Gaia*.

The g-modes have dominant tangential displacements, implying that their velocity at the limb of the star dominates the detected line-profile variability. Nevertheless, a common approach in the literature has been to rely on the ad hoc assumption that the radial and tangential components of the macroturbulent broadening profile are equal (Simón-Díaz & Herrero 2014). This is the reason why unrealistic, often supersonic values for the macroturbulent surface velocities are obtained. This in turn affects the estimation of the surface rotation (Aerts et al. 2014b). For that reason, it is essential to estimate the surface rotation first, independently from the macroturbulent broadening (Serebriakova et al. 2023).

In the following sections, we investigate *Gaia*'s capacity to shed light on the astrophysical cause(s) of the spectral-line broadening measured from RVS data. We do so for the two classes of γ Dor and SPB stars, whose velocity field at the stellar surface due to their non-radial oscillations is dominantly tangential (De Cat & Aerts 2002; Aerts et al. 2004).

5.1. Gaia DR3 line-broadening parameters

While *Gaia*'s medium-resolution RVS was not built to assess line broadening by stellar oscillations combined with rotation, it offers unprecedently large stellar samples analysed with a common methodology. We test the behaviour of line broadening measured with RVS with respect to the acting velocity fields at the stellar surface, where we know that our two

samples undergo the joint effect of time-independent rotational and time-dependent pulsational line broadening. To do so, we rely on two *Gaia* DR3 parameters used to measure spectral line broadening: `vbroad` (Frémat et al. 2023) and `vsini_esphs` (Creevey et al. 2023). Frémat et al. (2023) already carefully studied these two quantities to interpret spectral-line broadening for more than 33 million stars with $T_{\rm eff} \in [3.1; 14.5]$ kK. This range fully encapsulates that of our γ Dor sample and largely overlaps with the SPB sample.

The *Gaia* DR3 parameter `vbroad` captures the overall line broadening after deconvolving the spectra with the along-scan line spread function of *Gaia*'s RVS instrument (Sartoretti et al. 2022). This parameter `vbroad` therefore includes the joint effect of all possible astrophysical causes that give rise to spectral-line broading, such as oscillations, rotation, spots, turbulent convective velocities, and so on. The catalogued value of `vbroad` is the median value obtained by the multiple transit analysis (MTA) over at least six valid transits. The corresponding catalogued uncertainty is the standard deviation with respect to this median value. This implies that the uncertainty may be a measure of the line-profile variability, because its range captures the line broadening found from a minimum of six different epochs aside from the contribution of the noise. For the current study, we have `vbroad` measurements for 1775 of the 11636 γ Dor stars and for 190 of the 3426 SPB pulsators.

Another estimate of the RVS line broadening denoted as `vsini_esphs` is obtained by the so-called Extended Stellar Parametrizer module developed within the Astrophysical ParameterS Inferences System APSIS (Creevey et al. 2023). APSIS is able to treat the parameters of hot stars and delivers `vsini_esphs` as an intermediate data product. Its value approximates time-independent rotational broadening and was computed from the averaged values of BP and RP, and the averaged RVS spectrum. Although this leads to the variability being filtered out from the quantity `vsini_esphs` to some level, this latter still contains a contribution from the oscillations (cf., De Pauw et al. 1993, for the theoretical expression of the line width due to non-radial oscillations). Nevertheless, `vsini_esphs` is a cleaner measurement of the time-independent projected surface rotation velocity than `vbroad` when rotation dominates the spectral line broadening, as is the case for g-mode pulsators. The error published for `vsini_esphs` is an approximation of the statistical error and does not represent a measurement of the time-variable line broadening, as is the case for the standard deviation for `vbroad`. The quantity `vsini_esphs` deduced by APSIS results from an optimal RVS and BP/RP treatment for stars with a $T_{\rm eff}$ above 7500 K, while it relies on BP/RP alone for all stars with $T_{\rm eff} > 7000$ K, which were not observed by RVS. Values for `vsini_esphs` are available for 384 of the 11 636 γ Dor stars and for 1104 of the 3426 SPB stars.

The wavelength coverage of RVS was constructed so as to achieve optimal radial-velocity data for a broad range of stellar populations. Here we rely on its data for the purpose of studying spectral-line broading, for which the RVS wavelength domain is not optimal. This is particularly so for the hottest stars studied here. As a consequence, some of the `vbroad` and `vsini_esphs` measurements have large uncertainties. It is therefore essential to include these uncertainties, aside from the values themselves, in any proper astrophysical interpretation. We refer to Frémat et al. (2023) for a detailed and nuanced discussion about the quality of the `vbroad` and `vsini_esphs` measurements deduced from template spectra relying on the *Gaia* $T_{\rm eff}$ estimates. In particular, Frémat et al. (2023) discussed the correlations between these two parameters in detail for stars covering a broad range of

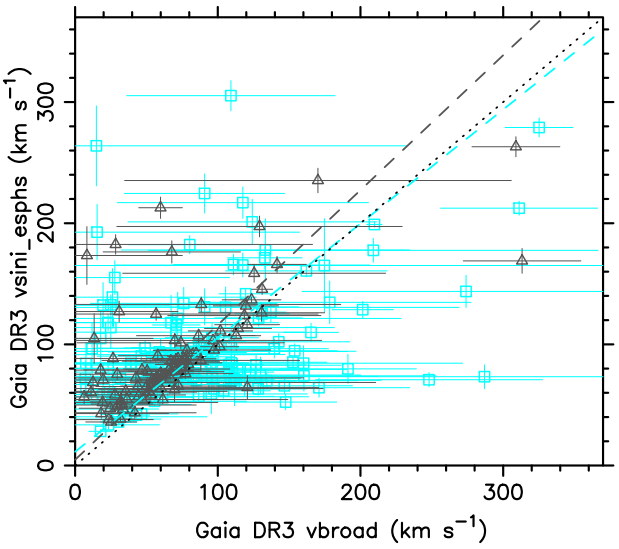

Fig. 7. Comparison between *Gaia* DR3 measurements of `vsini_esphs` and `vbroad` for the 100 γ Dor (grey triangles) and 156 SPB (cyan squares) stars for which both quantities are available. The full dotted line indicates the bisector, while the coloured dashed lines represent the best linear regression models for both samples.

magnitudes and temperatures. Of particular relevance for the current work is Fig. 16 in Frémat et al. (2023), illustrating two HR diagrams with density maps as a function of median `vbroad` values. That figure clearly reveals high `vbroad` values along the upper main sequence, where the γ Dor and SPB pulsators are situated (encompassing the p-mode-dominated class of δ Sct stars not treated here because of the much higher risk that their dominant frequency has an instrumental origin, as explained in Sect. 2). Their figure reveals higher `vbroad` values for hotter stars but the authors do not provide any formal quantitative comparisons between `vbroad` and the stellar parameters.

Figure 7 shows the 100 γ Dor and 156 SPB pulsators for which a measurement of both `vbroad` and `vsini_esphs` is available, along with their uncertainties. It can be seen that the overall range of the two quantities is roughly the same for these γ Dor and SPB stars. For each of the stars in Fig. 7, the two plotted quantities have similar yet not always equal values according to the uncertainty estimates. We reiterate that similarities between the two samples as a whole also occur for their ranges of the dominant mode amplitude and mode frequency (cf. Figs. 5 and 6). It is therefore natural to question whether the oscillation properties cause the time variability measured by `vbroad` and its standard deviation. On the other hand, we investigate whether the decrease in observed mode amplitude for faster rotators, as found in Paper I for the dominant p-modes of the *Gaia* DR3 δ Sct stars, also occurs for g-mode pulsators.

In what follows, we offer regression models accommodating errors in variables. This method allows us to include different measurements of the same astrophysical quantity (here the overall time-averaged spectral-line broadening) along with both star-specific and measurement-specific errors. These errors must be propagated properly when constructing the regression models and interpreting their outcome. This has been used in the context of *Gaia* data before; for example in a comparison between asteroseismic and astrometric parallaxes following DR1 (De Ridder et al. 2016). We first provide a general description of the methodology. Subsequently, we apply it to the sample of the 37 bona fide γ Dor stars. For all of these 37 stars we also have, in addition to their *Gaia* DR3 data, estimates of

their 'true' pulsational and rotational line broadening deduced from one homogeneous treatment of high-resolution high-S/N ground-based spectroscopy taken with one instrument (such homogeneous spectroscopic information is not available for all 26 bona fide SPB pulsators). We use the results obtained for the 37 bona fide γ Dor stars to treat the *Gaia* DR3 g-mode samples optimally, with the aim being to interpret their spectral-line broading properties.

5.2. Errors-in-variables model

Let us denote two observed quantities by Y_i and X_i and their true but unknown values by Y_i^* and X_i^*. The errors-in-variables model is then specified by:

$$Y_i = Y_i^* + \varepsilon_{Yi}, \tag{1}$$
$$X_i = X_i^* + \varepsilon_{Xi}, \tag{2}$$
$$Y_i^* = \beta_0 + \beta_1 X_i^* + \varepsilon_i, \tag{3}$$

with i indexing the stars in a sample. Here, β_0 and β_1 are fixed but unknown regression coefficients to be estimated from the data. The measurement error variances $\mathrm{var}(\varepsilon_{Yi}) = \sigma^2_{Yi}$ and $\mathrm{var}(\varepsilon_{Xi}) = \sigma^2_{Xi}$ are obtained from the observations. The residual error component ε_i, with variance σ^2, quantifies imperfection in the regression relationship.

If Y_i^* and X_i^* were almost identical, then the values of β_0 and β_1 would be expected to be close to 0 and close to 1, respectively. If the regression relationship in Eq. (3) is very precise relative to the measurement error, then the value of σ^2 would be near 0. Expressions (1)–(3) yield the mean and variance relationships:

$$E(Y_i) = \beta_0 + \beta_1 X_i, \tag{4}$$
$$\mathrm{Var}(Y_i) = \beta_1^2 \sigma^2_{Xi} + \sigma^2_{Yi} + \sigma^2. \tag{5}$$

Assuming (approximate) normality, a fully parametric specification follows, thus enabling maximum likelihood estimation:

$$Y_i \sim N(\beta_0 + \beta_1 X_i, \beta_1^2 \sigma^2_{Xi} + \sigma^2_{Yi} + \sigma^2). \tag{6}$$

The procedure `NLMIXED` developed by SAS Institute Inc. (2014) was used for the maximum likelihood estimation.

Extension to multiple predictors $X_{1i}, \ldots, X_{pi}$ is straightforward, upon replacing Eq. (6) by:

$$Y_i \sim N\left(\beta_0 + \sum_{j=1}^{p} \beta_j X_{ji}, \sum_{j=1}^{p} \beta_j^2 \sigma^2_{Xji} + \sigma^2_{Yi} + \sigma^2\right), \tag{7}$$

with obvious notation. It is convenient to write Eq. (7) in vector notation as:

$$Y_i \sim N(\boldsymbol{X}_i' \boldsymbol{\beta}, \boldsymbol{\beta}' \Sigma_{x,i} \boldsymbol{\beta} + \sigma^2_{Yi} + \sigma^2), \tag{8}$$

where $\boldsymbol{\beta} = (\beta_0, \beta_1, \ldots, \beta_p)'$ and $\Sigma_{x,i}$ is a diagonal matrix with $(0, \sigma^2_{X1i}, \ldots, \sigma^2_{Xpi})'$ along the diagonal.

A model-based prediction of Y_i^* and its standard deviation can be expressed as:

$$\widehat{Y_i^*} = \widehat{\beta}_0 + \sum_{j=1}^{p} \widehat{\beta}_j X_{ji}, \tag{9}$$

$$\widehat{\mathrm{s.d.}}(\widehat{Y_i^*}) = \sqrt{\widehat{\boldsymbol{\beta}}' \Sigma_{x,i} \widehat{\boldsymbol{\beta}} + \boldsymbol{x}_i' \widehat{\mathrm{var}}(\widehat{\boldsymbol{\beta}}) \boldsymbol{x}_i + \sigma^2_{Yi} + \widehat{\sigma^2}}, \tag{10}$$

where the unknown parameters have been replaced by their data-based estimates. Expressions (9)–(10) can be used to assess the quality of the model fit. The second term under the square root in Eq. (10) takes the uncertainty in the estimated regression coefficient into account.

5.3. Spectral-line broadening for the 37 bona fide γ Dor stars

For the 37 bona fide γ Dor stars, we now add three more quantities to the dominant frequency ν from *Kepler* photometry and the *Gaia* DR3 values for $\log T_{\rm eff}$, $\log g$, $\log(L/\mathcal{L}_\odot)$, and A_ν. Following their discovery as g-mode pulsators in the *Kepler* data, Tkachenko et al. (2013) set up a ground-based spectroscopic campaign with the HERMES spectrograph attached to the 1.2 m *Mercator* telescope situated at La Palma Observatory, Spain (Raskin et al. 2011). HERMES has a spectral resolution of 85000 and covers wavelengths from 377 to 900 nm. The HERMES spectra allowed Van Reeth et al. (2015) to deduce the overall spectral-line broading, here denoted as $\texttt{vbroad}_{\rm H}$, for the 37 stars and to unravel it into separate components stemming from time-independent rotational broadening ($v \sin i_{\rm H}$) and a broadening component due to the joint effect of microturbulence and the oscillation modes at the particular epoch of the observed spectrum. Microturbulence represents an artificial Gaussian line broadening needed to bring observed spectral lines into agreement with line predictions from one-dimensional atmospheric models. This small broadening is needed to take into account the occurrence of small-scale turbulent motions in the line-forming region that are not included in atmosphere models. On the other hand, the velocities due to non-radial g-mode oscillations result in time-dependent line broadening. In the case of γ Dor stars, their joint net effect in the line of sight is of the order of a few $\mathrm{km\,s^{-1}}$ (Aerts et al. 2004; De Cat et al. 2006). We therefore take the Gaussian line broadening determined by Van Reeth et al. (2015) as a good approximation for the overall pulsational broadening and denote it as $\texttt{vosc}_{\rm H}$.

The two quantities $v \sin i_{\rm H}$ and $\texttt{vosc}_{\rm H}$ were derived from the observed spectra after ensuring that none of the 37 stars are spectroscopic binaries. In practice, Van Reeth et al. (2015) found the following ranges for these two parameters for the sample of 37 stars: $\texttt{vosc}_{\rm H} \in [2.1; 4.7]\,\mathrm{km\,s^{-1}}$ and $\texttt{vsini}_{\rm H} \in [11; 170]\,\mathrm{km\,s^{-1}}$. The values and ranges reveal that this sample of bona fide γ Dor stars consists of slow to moderate rotators (compared to their breakup velocity) and that their rotational velocity is typically an order of magnitude greater than their tangential g-mode and microturbulent velocity together, where we recall that both quantities are integrations across the visible stellar surface in the line of sight. As these two velocity components influence the width of spectral lines added in quadrature, these ranges show that it is extremely challenging to unravel pulsational from rotational broadening, even for high-resolution spectroscopy (cf., Aerts et al. 2004, their Fig. 8). Moreover, as snapshot spectra cannot deliver proper time-dependent line-profile variations and only the line broadening is deduced, assuming a symmetrical line while ignoring its true shape, the relative uncertainties for $\texttt{vosc}_{\rm H}$ are considerable.

We use the 37 measured values for $\texttt{vbroad}_{\rm H}$, $v \sin i_{\rm H}$, and $\texttt{vosc}_{\rm H}$ to interpret the *Gaia* DR3 measurements of the overall line broadening (denoted as $\texttt{vbroad}_{\rm G}$ for the bona fide γ Dor stars), realising that the RVS resolving power is in principle insufficient to unravel pulsational from rotational line broadening. DR3 delivered $\texttt{vbroad}_{\rm G}$ for 27 of the bona fide γ Dor stars. We used these values to treat the following questions:

Table 1. Estimates (and standard errors) for the model parameters of the errors-in-variables model in Eq. (6) fitted to the bona fide γ Dor stars for four combinations of X and Y, where the HERMES quantities are available for all 37 stars and $\texttt{vbroad}_\mathrm{G}$ quantities are available for 27 of them.

	X	$\texttt{vbroad}_\mathrm{G}$	$\texttt{vbroad}_\mathrm{H}$	$\texttt{vsini}_\mathrm{H}$	$\texttt{vsini}_\mathrm{H}$
	Y	$\texttt{vbroad}_\mathrm{H}$	$\texttt{vbroad}_\mathrm{G}$	$\texttt{vbroad}_\mathrm{H}$	$\texttt{vbroad}_\mathrm{G}$
Effect	Par.	Estimates (s.e.)			
Intercept	β_0	4.8(2.4)	−2.5(2.5)	0.53(0.97)	−2.3(2.4)
Slope	β_1	1.02(0.04)	0.94(0.04)	0.99(0.02)	0.94(0.04)
Res. var.	σ^2	0.0000(0.0002)	0.0000(0.0000)	0.0000(0.0000)	0.0000(0.0000)
Effect	Par.	95% confidence intervals			
Intercept	β_0	[−0.16;9.74]	[−7.63;2.55]	[−1.44;2.49]	[−7.19;2.56]
Slope	β_1	[0.94;1.11]	[0.86;1.02]	[0.95;1.03]	[0.86;1.01]

1. Is the quantity $\texttt{vbroad}_\mathrm{G}$ obtained by *Gaia* RVS different from the independently obtained higher-precision quantities $\texttt{vbroad}_\mathrm{H}$ or $\texttt{vsini}_\mathrm{H}$?

2. Can the variability in $\texttt{vbroad}_\mathrm{H}$ measured from HERMES for the sample of the 37 bona fide γ Dor stars be predicted by the *Gaia* DR3 covariates $\log T_\mathrm{eff}$, $\log g$, $\log(L/\mathcal{L}_\odot)$, ν, and A_ν and if so what is the quality of their predictive power?

Answering these two questions will help us to find an astrophysical interpretation of *Gaia*'s vbroad values for the two new large samples of g-mode pulsators, circumventing the need for measurements of line broadening deduced from high-resolution spectroscopy, as such measurements are only available from a homogeneous data analysis for the 37 bona fide γ Dor pulsators.

To tackle the first question, we fit the statistical model in Eq. (6) for four combinations of X and Y. The parameter estimates and statistical properties of the regression models are presented in Table 1. We find that the residual variances σ^2 are all extremely close to zero. None of the intercepts are significantly different from zero, and none of the slopes are significantly different from unity. This implies that all three quantities are essentially equal to each other within the uncertainty limits specified by the measurement errors. The fractions of the variance explained by each of the four models range from 94% to 100%.

Given that $\texttt{vbroad}_\mathrm{G}$ is missing for 10 of the 37 γ Dor stars, the models involving this variable were refitted after multiple imputation (Molenberghs & Kenward 2007) to examine the potential impact of missingness on the results. This well-known statistical technique was only recently introduced in astrophysics for the treatment of missing data; for example, in the multivariate stellar astrophysics study relating nine measured quantities to surface nitrogen by Aerts et al. (2014a) and the time-series analysis of visual binaries by Claveria et al. (2019). The method was applied here as follows. First, based on a so-called imputation model, 100 copies of each missing value are drawn from the predictive distribution of what is missing given what is observed. Second, each dataset completed in this way is then analysed with the model that would have been used had the data been complete. Third, the 100 results combined into a single result using appropriate combination rules. Results were qualitatively very similar to those reported in Table 1, giving us confidence that these missing data do not play an important role in the relationships presented in Table 1. For this reason and simplicity, we proceed with the results presented in Table 1.

Following up on the study by Van Reeth et al. (2015), we conclude from the bona fide γ Dor g-mode pulsators that single epoch spectra, although of high resolution and high S/N, cannot be used to distinguish the overall line broadening from the line broadening caused solely by rotation when working with a fudge parameter relying on the assumption of a time-independent symmetrical line profile. Given this spectral line modelling limitation, we find that *Gaia* RVS delivers good approximate values for spectral-line broading compared to those deduced from snapshot high-resolution spectroscopy for early F-type stars. Nevertheless, the uncertainties deduced from the HERMES spectra are lower, because its more suitable spectral coverage includes more spectral lines whose shape is determined by the temperature rather than pressure broadening.

Table 2. Estimates (standard errors) for the model parameters of the errors-in-variables model for $\texttt{vbroad}_\mathrm{H}$, fitted to the bona fide γ Dor stars based on backward selection from a set of predictors.

Effect	Par.	Est. (s.e.)	p-value	95% conf. int.
Intercept	β_0	95(4)		[86;104]
$100\cdot(\log T_\mathrm{eff}-3.85)$	β_1	−28(5)	<0.0001	[−37;−18]
$\log g - 4.0$	β_2	60(14)	0.0001	[32;88]
$\nu - 1.75$	β_3	57(6)	<0.0001	[44;70]
Res. var.	σ^2	70(152)	0.3623	[−238;378]

To address the second question outlined above, we examine the effect of the *Gaia* DR3 variables $\log(L/\mathcal{L}_\odot)$, $\log T_\mathrm{eff}$, $\log g$, A_ν, and ν on the independently obtained parameter $\texttt{vbroad}_\mathrm{H}$. This can be done with or without adding $\texttt{vbroad}_\mathrm{G}$ and with or without adding $\texttt{vosc}_\mathrm{H}$ to the set of predictors. We proceed by backward selection, starting with the full set of predictors and then progressively removing the one with the highest p-value, until only significant effects remain (i.e. all $p \leq 0.05$). In both versions with $\texttt{vbroad}_\mathrm{G}$ included in the predictor set, this is the only one remaining after model selection, and we recover the result already reported in Table 1, as expected.

When $\texttt{vbroad}_\mathrm{G}$ cannot be considered, as is the case for the majority of *Gaia* targets, the following insignificant predictors are removed by means of backward selection: first A_ν, second $\log(L/\mathcal{L}_\odot)$, and third $\texttt{vosc}_\mathrm{H}$. As the latter variable is removed, whether or not it is included among the predictors to select from is not important. Hence, only one additional model is obtained, the fit of which is presented in Table 2. This model explains about 58% of the variance present in $\texttt{vbroad}_\mathrm{H}$ via the effective temperature, surface gravity, and dominant frequency as covariates, which are all delivered by *Gaia* DR3. We note that the ranges of the covariates are [3.83; 3.87] for $\log T_\mathrm{eff}$, [3.71; 4.48] for $\log g$, and [0.78; 3.01] day^{-1} for ν, which is why they were linearly transformed as displayed in Table 2 to optimally stabilise the model fit.

Table 3. Estimates (standard errors) for the model parameters of the errors-in-variables model, relating `vbroad` to `vsini_esphs`, on the 100 completers within the *Gaia* DR3 set of γ Dor stars.

Effect	Par.	Estimate (s.e.)	p-value	95% conf. int.
Intercept	β_0	−5(3)		[−12;2]
Slope	β_1	0.90(0.05)	<0.0001	[0.81;0.99]
Res. var.	σ^2	0(4)	0.98	[−7;7]

In response to the second question, we find the dominant g-mode frequency ν to be a significant predictor of the high-resolution spectroscopic line broadening, alongside the temperature and gravity of the star. This offers the opportunity to predict the line broadening for all the *Gaia* γ Dor stars without a *Gaia* measurement of the line broadening if these three covariates are available, as is the case for the majority of the *Gaia* DR3 γ Dor stars. Of course it should be borne in mind that some predictors exhibit mild to strong correlation, given their astrophysical meaning. In the particular application of the bona fide γ Dor stars, the strongest correlation among the predictors is the one between $\log(L/\mathcal{L}_\odot)$ and $\log g$, namely –0.70. The correlation between $\log T_{\rm eff}$ and A_ν is 0.40, while ν correlates equally with $\log T_{\rm eff}$ and with $\log g$ with a moderate value of 0.32. All other correlations are much smaller. Hence, the regression coefficients in a model with multiple predictors should be interpreted as the effect of change by one unit in a predictor, while all others remain constant, in this case for the three surviving predictors $\log T_{\rm eff}$, $\log g$, and ν. A graphical perspective on the predictions for $\texttt{vbroad}_{\rm H}$ from $\texttt{vbroad}_{\rm G}$, $\texttt{vsini}_{\rm H}$, and the three covariates is shown in Fig. 8 using Eqs. (9)–(10).

5.4. Results for the Gaia DR3 γ Dor pulsators

Armed with the knowledge that $\texttt{vbroad}_{\rm G}$ and $\texttt{vbroad}_{\rm H}$ are equal for the 37 bona fide γ Dor stars to within their measurement uncertainties from high-resolution and *Gaia* RVS spectra, and with the predictive model for these quantities given in Table 2, we now look at the sample of 11 636 *Gaia* DR3 γ Dor stars. For all of those, full information is available on $\log T_{\rm eff}$, $\log g$, $\log(L/\mathcal{L}_\odot)$, ν, and A_ν, deduced in one homogeneous way from *Gaia* DR3 following Paper I. For 100 of these stars, both $\texttt{vbroad}_{\rm G}$ (hereafter simplified to `vbroad`) and `vsini_esphs` are recorded. These are the so-called completers of the *Gaia* DR3 γ Dor stars. For 1775 γ Dor stars, there is a measurement on `vbroad` but not on `vsini_esphs`, and for 384 γ Dor stars, `vsini_esphs` information is available but `vbroad` is missing. For the remaining 9577 stars, both of these line broadening quantities are missing.

When considering the 100 completers only, we again conclude that `vbroad` and `vsini_esphs` are identical within the bounds specified by the measurement errors given that the slope parameter is roughly equal to unity and the residual variance is not different from zero (see Table 3). Figure 7 shows that the two variables `vbroad` and `vsini_esphs` are similar for the γ Dor stars with both estimates, while graphically revealing the different meaning of their uncertainty regions. The grey dashed line in that figure represents the regression model in Table 3.

For the full *Gaia* DR3 γ Dor data set, the relationship between `vbroad` and `vsini_esphs` can also be assessed using all stars after performing multiple imputation. For this application, we drew ten imputations using information on `vbroad`, `vsini_esphs`, their standard errors, and the covariates $\log T_{\rm eff}$, $\log g$, $\log(L/\mathcal{L}_\odot)$, ν, and A_ν. Given that complete information is available for less than 1% of stars, the relationship found from multiple imputation is relatively different from that found for the 100 completers. This is not surprising given the relatively large uncertainties on the two broadening parameters and the fact that they are rather weakly correlated with other information in the

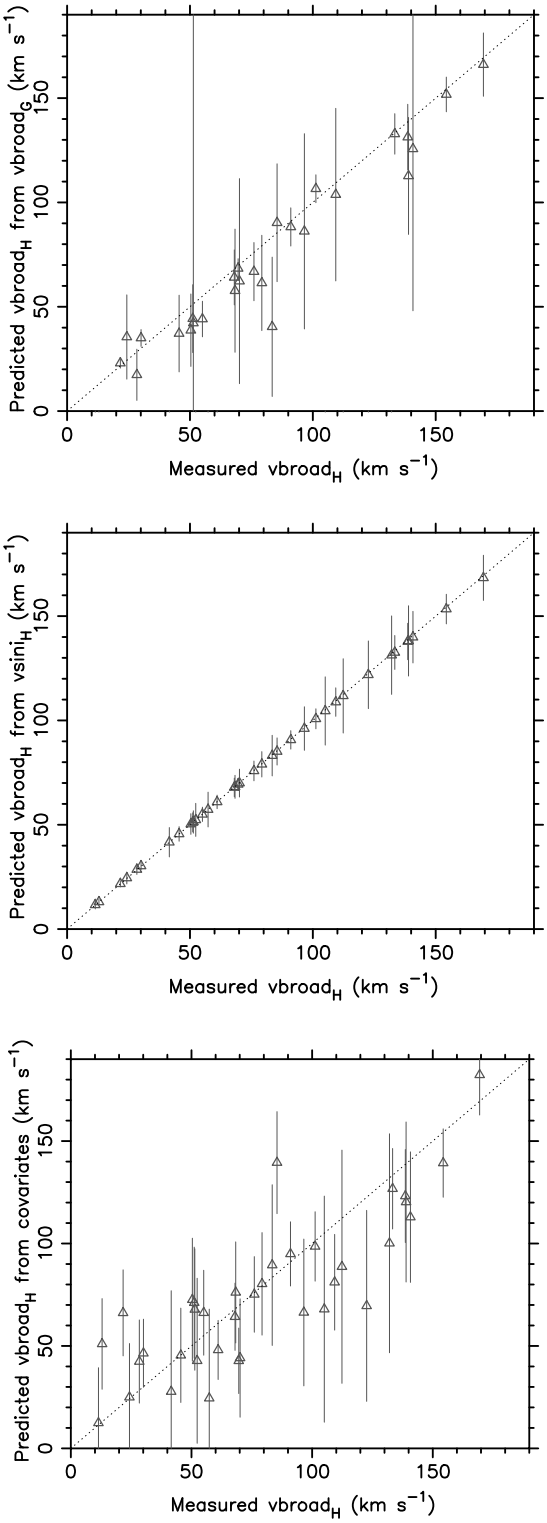

Fig. 8. Quality of predictions of $\texttt{vbroad}_{\rm H}$ by $\texttt{vbroad}_{\rm G}$ (upper panel), $\texttt{vsini}_{\rm H}$ (middle panel), and the set of covariates (lower panel) for the 37 bona fide *Kepler* γ Dor stars. The vertical bars are defined by the predicted value ± its standard deviation based on the errors-in-variables models in Table 2.

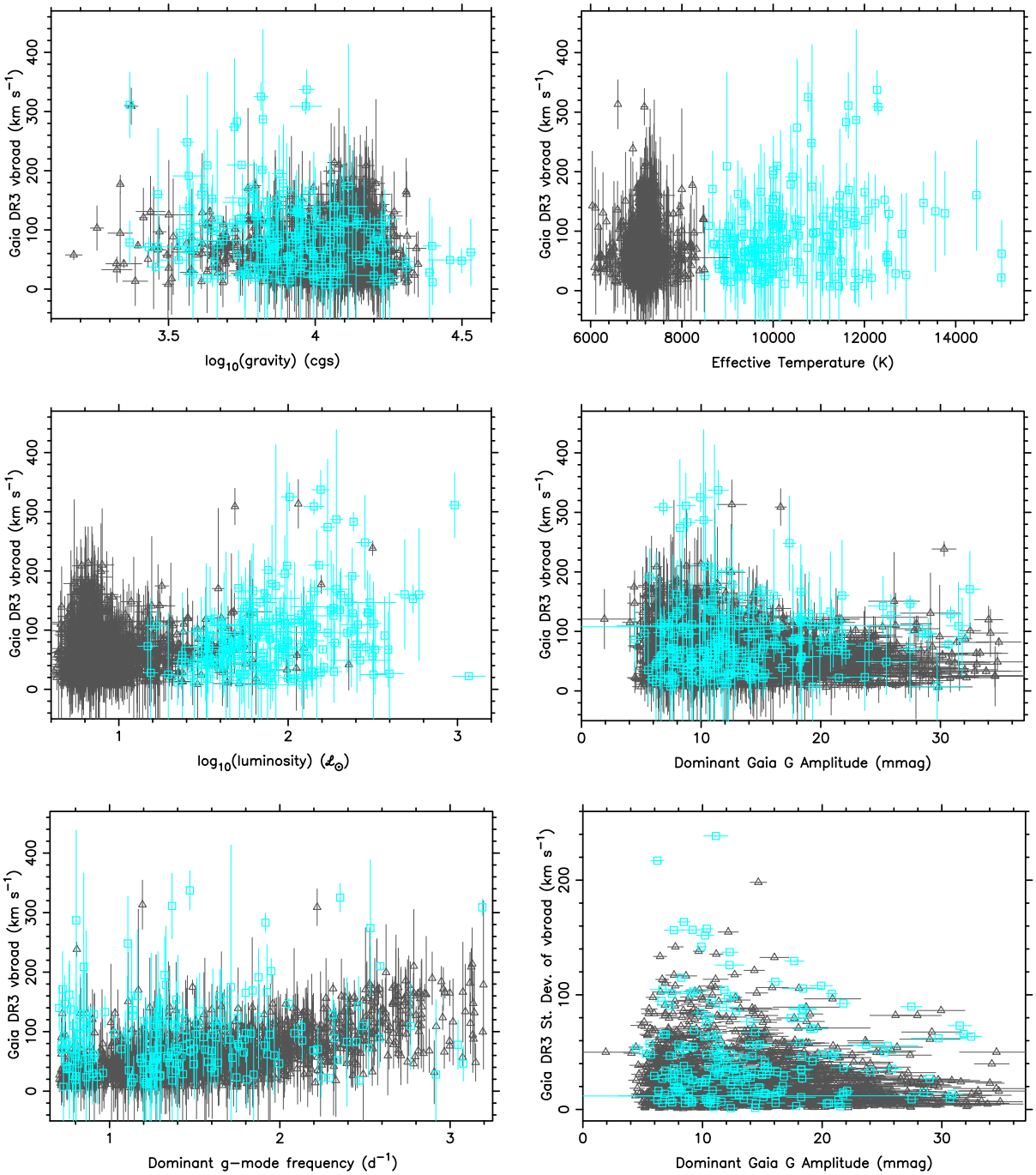

Fig. 9. *Gaia* DR3 measurements of `vbroad` versus each of the five covariates as indicated for the 1775 γ Dor (grey triangles) and 190 SPB (cyan squares) stars having these quantities available. The lower right panel shows the standard deviation of `vbroad` as a function of the dominant g-mode amplitude. When invisible, the errors are smaller than the symbol sizes.

dataset. Moreover, the very large fraction of incomplete information destabilises the inference from multiple imputation. These issues taken together suggest that the results of multiple imputation are too unstable to provide trustworthy results. For these reasons, the subsequent analysis is based on completers only for each of the regression applications discussed below.

We now turn to the relationship between `vbroad` and the predictor variables, applying backward selection to the errors-in-variables model for the 1775 γ Dor stars for which this quantity and the covariates $\log T_{\rm eff}$, $\log g$, $\log(L/\mathcal{L}_\odot)$, ν, and A_ν are available (whose regression coefficients we denote as $\beta_1,\beta_2,\beta_3,\beta_4,\beta_5$, respectively). It turns out that all these covariates are significant except the amplitude of the dominant frequency, which has a p-value of 0.0662 and is therefore borderline significant. This is why we present the regression models with and without this covariate in Table 4. Both these models explain 42% of the variance in the measurements of `vbroad`. It can be seen in Table 4 that keeping A_ν in the model does not alter the regression coefficients of the other four covariates. We show the measurements of `vbroad` as a function of each of the covariates in Fig. 9.

As discussed in Sect. 5.1, `vsini_esphs` is based on the averaged BP/RP (and averaged RVS spectrum when available) and therefore has smaller uncertainty than `vbroad` whose

Table 4. Estimates (standard errors) for the parameters of the errors-in-variables model for `vbroad` for the 1775 *Gaia* DR3 γ Dor stars with measured values for this quantity, based on backward selection from the set of listed predictors.

Effect	Par.	Estimate (s.e.)	p-value	95% conf. int.
		With A_V		
Intercept	β_0	−478(262)		[−993;−36]
log $T_{\rm eff}$	β_1	238(87)	0.0065	[67;409]
log g	β_2	−100(19)	<0.0001	[−138;−63]
log $(L/\mathcal{L}_\odot)$	β_3	−45(15)	0.0022	[−74;−16]
ν	β_4	44(1)	<0.0001	[41;46]
A_V	β_5	−192(104)	0.0662	[−397;13]
Res. var.	σ^2	397(20)	<0.0001	[358;437]
		Without A_V		
Intercept	β_0	−478(260)		[−988;−32]
log $T_{\rm eff}$	β_1	237(87)	0.0062	[68;407]
log g	β_2	−100(19)	<0.0001	[−138;−63]
log $(L/\mathcal{L}_\odot)$	β_3	−45(15)	0.0023	[−73;−16]
ν	β_4	44(1)	<0.0001	[41;47]
Res. var.	σ^2	395(20)	<0.0001	[356;435]

Notes. Both models explain 42% of the variance in `vbroad`.

Table 5. Estimates (standard errors) for the parameters of the errors-in-variables model for `vsini_esphs` for the 384 *Gaia* DR3 γ stars with measured values for this quantity based on backward selection from a set of predictors.

Effect	Par.	Estimate (s.e.)	p-value	95% conf. int.
Intercept	β_0	198(56)		[88;308]
log g	β_2	−37(15)	0.0161	[−66;−7]
ν	β_4	17(6)	0.0047	[5;28]
Res. var.	σ^2	599(152)	0.0002	[296;901]

uncertainty interval represents the time-dependent line broadening covered by at least six snapshot spectra. By construction, `vsini_esphs` is expected to be a better representative of the time-independent surface rotation velocity of the star than `vbroad`. Indeed, the latter quantity approximates the overall time-dependent spectral-line broading due to various phenomena acting together because it was computed as the median value from individual transits taken at different epochs and treated as such by the MTA.

To test whether or not `vsini_esphs` and `vbroad` indeed capture different astrophysical information, we repeat the same backward model selection for `vsini_esphs`, considering the same covariates for the 384 γ Dor stars with a measurement of `vsini_esphs`. This leads to the successive removal of A_V, $\log(L/\mathcal{L}_\odot)$, and log $T_{\rm eff}$, as these are found to be insignificant. The coefficients of the resulting regression model are listed in Table 5, while the plots of the measurements of `vsini_esphs` as a function of each of the covariates are included in Appendix A (Fig. A.1, to be compared with Fig. 9). We find that `vsini_esphs` does not depend on the effective temperature or the luminosity, while the surface gravity and dominant frequency remain significant covariates. These two covariates offer the same dependence for `vsini_esphs` as for `vbroad`, that is, lower log g (a more evolved star) and higher ν give larger line broadening. Regarding ν, this is well understood in terms of an asteroseismic interpretation and in agreement with the findings based on the HERMES spectroscopy by Van Reeth et al. (2015) for the bona fide γ Dor stars. Indeed, a higher dominant g-mode frequency in the inertial frame of an observer corresponds to a faster rotating star (Van Reeth et al. 2015, 2016; Pápics et al. 2017, for galleries of *Kepler* light curves and frequency spectra as a function of rotation frequency). Hence, higher asteroseismic ν is a signature of faster stellar rotation and thus of larger line broadening, irrespective of whether one considers `vsini_esphs` or `vbroad`.

While the resulting regression model for `vsini_esphs` of 384 class members explains only 5% of the variance in that quantity, the regression model for `vbroad` based on the 1775 stars for which this quantity is available explains 42% of the measured variance. Therefore, the time-independent projected rotational velocity represented by `vsini_esphs` of the γ Dor stars is independent of their effective temperature and luminosity while being only weakly dependent on their gravity. On the other hand, the time-dependent quantity `vbroad` does connect to the effective temperature of the γ Dor stars, such that the hotter the star, the larger `vbroad`. Our astrophysical interpretation of these findings connects well to the excitation mechanisms and to the level of line broadening found for γ Dor stars in the literature. Indeed, as the *Kepler* data allow for detailed asteroseismic modelling, we know that the dominant modes of the bona fide g-mode pulsators are dipole prograde modes and that these stars occupy a narrow range in mass, namely [1.3; 1.9] $M_\odot$, while they cover the entire main sequence (Mombarg et al. 2019, 2021). This pulsation class therefore has stars with a relatively broad range of log g and radii (cf. Fig. 4). The variability in log $T_{\rm eff}$ and log g revealed among the class members is therefore mainly a signature of evolutionary status.

The regression models for `vbroad` and `vsini_esphs` reveal stars that are more evolved have larger spectral-line broading, while maximal time-dependent line broadening occurs for $T_{\rm eff}$ between 6500 and 7500 K (cf. the grey triangles in the upper left panel of Fig. 9). This is precisely the temperature range where Grassitelli et al. (2015a) found a maximal effect of turbulent pressure in the stellar envelope of evolved A- and F-type dwarfs, offering an additional mechanism to excite high-order eigenmodes in such objects, aside from the classical κ mechanism active in the hotter γ Dor stars and flux blocking at the bottom of the convective envelope causing such g-modes in the cool class members (Guzik et al. 2000; Dupret et al. 2005; Xiong et al. 2016). In addition, Tkachenko et al. (2020) already showed that ignoring the turbulent pressure in stellar atmosphere models affects the estimation of microturbulent broadening and results in an overestimation of the effective temperature by a few percent. Moreover, the authors found this effect to become more pronounced as the star evolves, that is for decreasing log g. We therefore conclude to have found observational evidence from *Gaia* DR3 `vbroad` measurements that time-dependent macroturbulent spectral-line broading in these stars is connected with their excited g-modes and/or surface gravity, in addition to surface rotation. The amplitude limitation from *Gaia* DR3 and the comparative distributions of the dominant amplitudes and frequencies between the *Gaia* DR3 and bona fide γ Dor pulsators (cf. left panels of Figs. 5 and 6) suggest that the detected dominant frequencies are due to large-scale (i.e. low-degree) gravito-inertial modes. The interplay of the dominant g-mode with the rotation of the star, along with variability in log $T_{\rm eff}$ and log g due to poor treatment of turbulent pressure in the line-forming region, explain the overall spectral-line broading estimates from *Gaia* DR3.

Table 6. Estimates (standard errors) for the model parameters of the errors-in-variables model, relating `vbroad` to `vsini_esphs`, on 156 completers within the SPB sample.

Effect	Par.	Estimate (s.e.)	p-value	95% conf. int.
Intercept	β_0	−11(5)		[−20;−2]
Slope	β_1	1.06(0.05)	<0.0001	[0.97;1.15]
Res. var.	σ^2	25(30)	0.41	[−35;84]

We point out that the regression model for `vbroad` in Table 4 explains 42% of the measured variance in the spectral-line broading, while the corresponding regression model found for the bona fide pulsators explained 58% of their measured variance. Both these results are readily understood given that we are dealing with multi-periodic g-mode pulsators. Indeed, γ Dor pulsators have tens of high-order low-degree g-modes active simultaneously, irrespective of which of the three excitation mechanisms is dominant (Van Reeth et al. 2015). The line broadening captures the collective effect of all these modes together (Aerts et al. 2009). Nevertheless, the frequencies of the excited g-modes in addition to the dominant one were not included in the regression model because the *Gaia* light curves currently do not provide sufficient data to unravel the multi-periodic oscillations active in these stars. While the frequencies and amplitudes of the second strongest variability signal were determined in Paper I, it was found that a relatively large number of those frequencies cannot be distinguished from frequencies above 3 day^{-1} that may result from instrumental effects. That is why we did not use these secondary frequencies from DR3. It is anticipated that improved regression models explaining a higher fraction of the variance in the spectral line broadening will become possible from DR4 and particularly DR5, because the longer time base and doubling of the number of epochs in the *Gaia* photometry will allow several additional g-mode frequencies to be elucidated, particularly when combined with additional light curves dedicated to asteroseismology as illustrated from combined HIPPARCOS and TESS or ground-based data (cf. Waelkens et al. 1998; De Cat et al. 2007; Cuypers et al. 2009). Still, *Gaia*'s sampling is too sparse to deliver all the modes active in these multi-periodic g-mode pulsators, while they do contribute to the overall broadening of the spectral lines (cf. Mathias et al. 1994, for the theoretical expression of the spectral line width due to multi-periodic non-radial oscillations). The fraction of the variance explained by regression models relying on the fundamental parameters and the significant frequencies in *Gaia* light curves will therefore always be limited, even for the bona fide class members. In this sense, the 42% reached for the model in Table 4 is high.

5.5. Results for the Gaia DR3 SPB pulsators

We now repeat the same analyses for the 3426 new *Gaia* DR3 SPB stars. Among these, both `vbroad` and `vsini_esphs` are recorded for 156 stars. For 34 of them, there is a measurement on `vbroad` but not on `vsini_esphs`, while for 948 stars, `vsini_esphs` is available but `vbroad` is missing. For the remaining 2288 SPB stars, both of these are missing. In line with the arguments provided in Sect. 5.4, we now restrict our attention to an analysis of the completers to test relationships for `vsini_esphs` and `vbroad`.

We tested whether or not the two measures for the spectral line broadening are equal; the results are given in Table 6 and shown graphically in Fig. 7 (cyan symbols). Just like for the *Gaia* DR3 γ Dor sample, we again see a relationship that is consistent with the hypothesis that `vbroad` and `vsini_esphs` are identical, keeping in mind the errors for `vsini_esphs` and the standard deviation for `vbroad`.

Table 7. Estimates (standard errors) for the model parameters of the errors-in-variables model for `vbroad` of the 190 SPB stars for which a measurement of this quantity is available based on backward selection from the set of predictors.

Effect	Par.	Estimate (s.e.)	p-value	95% conf. int.
Intercept	β_0	−2764(643)		[−4033;−1495]
log $T_{\rm eff}$	β_1	963(219)	<0.0001	[532;1395]
log g	β_2	−213(51)	<0.0001	[−312;−113]
log$(L/\mathcal{L}_\odot)$	β_3	−109(42)	0.0105	[−192;−26]
ν	β_4	34(8)	0.0001	[19;50]
A_ν	β_5	−1492(715)	0.0384	[−2903;−81]
Res. var.	σ^2	1909(300)	<0.0001	[1317;2501]

Notes. The model explains 21% of the variability in the data.

Next, the relationship between `vbroad` and the candidate predictors is examined relying on the 190 SPB stars for which these data are available, once again applying backward selection to the errors-in-variables model. All covariates are again significant. The regression model in Table 7 explains 21% of the variance in `vbroad`. Backward selection applied to `vsini_esphs` for the 1104 SPB stars with this quantity reveals $T_{\rm eff}$ and ν to be significant predictors, with a regression model explaining 8% of the variance (see Table 8). For the regression coefficient of ν, we assign the same astrophysical interpretation as before, namely that higher ν corresponds to faster surface rotation, following the SPB studies by Pápics et al. (2017), Pedersen et al. (2021), and Pedersen (2022b).

As for the role of the effective temperature in `vbroad` and `vsini_esphs`, Pápics et al. (2017) already found evidence that hotter SPB stars are more massive and tend to rotate faster. The $T_{\rm eff}$ dependence revealed is therefore, in the first instance, a dependence on stellar mass rather than on stellar evolution, as we found for the γ Dor stars. This result is as expected, given that SPB stars cover a factor 3 in mass, from 3 $M_\odot$ to 9 $M_\odot$. Pedersen et al. (2021) placed the observed properties of the 26 bona fide *Kepler* SPB stars included here and those studied from the ground by De Cat & Aerts (2002) into the context of stellar evolution theory. This showed large diversity of ν and A_ν in terms of the spectroscopic log $T_{\rm eff}$ and log g, as well as log$(L/\mathcal{L}_\odot)$ from *Gaia* DR2. This diversity was interpreted as due to the range in mass and rotation rate, the latter covering from almost zero to almost critical rotation for the *Kepler* sample (Aerts et al. 2021; Pedersen 2022b). Despite the limited predictive power of the regression model in Table 7, it reveals that larger line broadening occurs for hotter and/or more evolved SPB stars with higher dominant g-mode frequencies (cf. Fig. 9). This highlights that hotter, younger stars have faster rotation, shifting their g-modes further into the gravito-inertial regime of the frequency spectrum than those of slower rotators (see Aerts et al. 2019, for a discussion of the various frequency regimes of waves connected to the dominant restoring forces).

The luminosity, log$(L/\mathcal{L}_\odot)$, now also has a significant contribution as a predictor for `vbroad` with a $p-$value of 0.0105. The model reveals that less luminous SPB stars have higher line broadening but its regression coefficient is not very accurate. Moreover, the sample of SPB stars with a measurement of `vbroad` is an order of magnitude smaller than for the γ Dor stars

Table 8. Estimates (standard errors) for the model parameters of the errors-in-variables model for `vsini_esphs` based on the 1104 SPB stars in the sample for which a measurement for this quantity is available based on backward selection from a set of predictors.

Effect	Par.	Estimate (s.e.)	p-value	95% conf. int.
Intercept	β_0	−573(319)		[−1204;58]
log $T_{\rm eff}$	β_1	157(80)	0.0496	[0;315]
ν	β_4	20(6)	0.0016	[8;32]
Res. var.	σ^2	745(154)	<0.0001	[442;1049]

Notes. The model explains 8% of the variability in the data.

and is skewed towards low-mass class members, limiting this interpretation to only a small part of the SPB instability region. This is graphically illustrated in Fig. 9, where trends reveal that more evolved and more luminous SPB stars have higher `vbroad` but are not sufficiently well represented in membership to have an effect on the regression model as important as that of the cool class members. Moreover, the luminosity panel in Fig. 9 reveals more of a quadratic than a linear trend for the SPB stars. As already highlighted above, and as opposed to the γ Dor stars, the luminosity of SPB pulsators is mostly determined by their mass rather than by their evolutionary stage, which is the case for the γ Dor stars. This, along with the relatively large scatter in log g and in effective temperature, as well as the lower fraction of the variance explained by the linear regression model for `vbroad`, makes the distillation of a simple astrophysical interpretation for `vbroad` more difficult for SPB stars. This conclusion is by itself fully in line with the diversity in pulsational behaviour occurring in the *Kepler* sample of bona fide SPB pulsators (Pedersen et al. 2021; Pedersen 2022a).

Finally, we stress that time-dependent macroturbulent spectral-line broadening due to the g-modes of SPB pulsators has already been found in several of the brightest class members (Aerts et al. 2014b), with values in agreement with those found here for the new faint *Gaia* DR3 class members. Moreover, the density of modes excited by the κ mechanism peaks in the lower part of the instability strip, near 13 000 K (Pápics et al. 2017). These pulsators have a mass regime where the interpretation of turbulent pressure exciting extra high-order g-modes in addition to the classical κ mechanism does not hold (Grassitelli et al. 2015b). Macroturbulence in these pulsators has already been established as a time-independent downgraded quantity representing their dominant tangential pulsational velocity by Aerts et al. (2009, 2014a).

6. Discussion and conclusions

Thanks to the homogeneous treatment of its multitude of observations and its large-scale survey capacity, the *Gaia* mission has the potential to play a significant role in gravito-inertial asteroseismology. First of all, its photometric light curves allow the discovery of thousands of new g-mode pulsators belonging to the classes of the γ Dor and SPB stars. Secondly, its broadening parameter `vbroad` contains astrophysical information on stellar oscillations with mmag-level observed amplitudes. We found these results after reassigning a fraction of 22% of the γ Dor candidates as SPB pulsators according to their effective temperature, which is above 8500 K, a property not taken into account in the variability classifications used in Paper I.

We find the two samples of new *Gaia* DR3 g-mode pulsators to have similar fundamental parameters to those of bona fide class members, although the *Gaia* SPB pulsators only cover the cooler and less massive class members. We studied the astrophysical properties of the new γ Dor and SPB pulsators from regression models built upon the principle of errors-in-variables, with their fundamental parameters and dominant oscillation properties as predictors of the overall spectral-line broading. The *Gaia* DR3 quantity `vsini_esphs` offers a good estimate of the overall time-independent spectral-line broadening, reflecting that the surface rotation of the stars in our samples is the dominant line-broadening mechanism. All regression models reveal the dominant g-mode frequency to be a significant predictor of the *Gaia* DR3 `vbroad` parameter and its standard deviation, which together represent the overall time-dependent spectral-line broading.

We explicitly checked via reanalyses of all regression models that none of the astrophysical interpretations change if we use the effective temperature of 9500 K as a threshold for the reclassifications among the γ Dor and SPB candidates. Such a threshold temperature is based on instability computations by Szewczuk & Daszyńska-Daszkiewicz (2017) for the cool border of Galactic rotating SPB stars instead of the adopted 8500 K based on the hot border for the γ Dor instability strip by Xiong et al. (2016). We find from the upper left panel of Fig. 9 that *Gaia* DR3 shows 9500 K to be a less natural and more abrupt threshold temperature between the two classes than the adopted 8500 K. Nevertheless, using 9500 K still leads to compliance of class populations with the IMF and almost all the coefficients obtained for the regression models remain within the uncertainty ranges listed in the tables we provide here using 8500 K as a threshold.

Despite the limiting resolution of the RVS spectroscopy, the line broadening of rotating g-mode pulsators offered by *Gaia* is in full agreement with results of well-known class members observed with high-precision space photometry and high-resolution spectroscopy. In particular, we find the dominant g-mode frequency to be a significant predictor of the overall line broadening. This supports earlier findings that macroturbulence is merely a simplified time-independent approximation of the true velocity fields at the stellar surface that cause line-profile variability for g-mode pulsators (Aerts et al. 2014b). We conclude that the combined effect of surface rotation and tangential velocities resulting from multi-periodic g-modes can be estimated from `vbroad` for the case of main sequence stars of intermediate mass. The regression models for `vbroad` are fully in line with various excitation predictions for g-modes in γ Dor and SPB pulsators.

Given that the regression models based on the fundamental parameters and on the dominant pulsation mode presented in Sect. 5 explain part of the variability of `vbroad`, it is sensible to also consider the standard deviation of `vbroad` as a measured quantity and to check whether or not its variance can be predicted by any of the covariates. Indeed, aside from being caused by noise, this quantity may partially represent the time-dependence of the line broadening. From our regression analyses (presented in Appendix B), we conclude that the noise contribution to the standard deviation of `vbroad` is dominant over intrinsic line-profile variability for the γ Dor pulsators. For the SPB stars, the standard deviation of `vbroad` is related to their surface rotation, effective temperature, and g-mode frequency at the level of 20% variance reduction for the regression model based on these three covariates.

Finally, we conclude that our analyses of ~15 000 new *Gaia* DR3 g-mode pulsators bring the qualitative results on `vbroad` by Frémat et al. (2023) into full agreement with

our quantitative assessments of macroturbulence in g-mode pulsators, as already suggested by the simulation study in Aerts et al. (2009).

Acknowledgements. The research leading to these results has received funding from the KU Leuven Research Council (grant C16/18/005: PARADISE). CA and JDR acknowledge support from the BELgian federal Science Policy Office (BELSPO) through a PRODEX grant for the ESA space mission *Gaia*. CA acknowleges financial support from the Research Foundation Flanders under grant K802922N (Sabbatical leave). CA and GM are grateful for the kind hospitality offered by the staff of the Center for Computational Astrophysics at the Flatiron Institute of the Simons Foundation in New York City during their work visit in the fall of 2022. The authors thank the referee for the suggestion to investigate the sensitivity of the results to the temperature treshold used to reclassify the g-mode pulsators. They also acknowledge Dominic Bowman and Andrew Tkachenko for valuable comments which helped to improve the manuscript.

References

Aerts, C. 2021, Rev. Modern Phys., 93, 015001
Aerts, C., & De Cat, P. 2003, Space Sci. Rev., 105, 453
Aerts, C., & Rogers, T. M. 2015, ApJ, 806, L33
Aerts, C., De Pauw, M., & Waelkens, C. 1992, A&A, 266, 294
Aerts, C., De Cat, P., Peeters, E., et al. 1999, A&A, 343, 872
Aerts, C., Cuypers, J., De Cat, P., et al. 2004, A&A, 415, 1079
Aerts, C., Puls, J., Godart, M., & Dupret, M. A. 2009, A&A, 508, 409
Aerts, C., Christensen-Dalsgaard, J., & Kurtz, D. W. 2010, Asteroseismology (Heidelberg: Springer-Verlag)
Aerts, C., Molenberghs, G., Kenward, M. G., & Neiner, C. 2014a, ApJ, 781, 88
Aerts, C., Simón-Díaz, S., Groot, P. J., & Degroote, P. 2014b, A&A, 569, A118
Aerts, C., Molenberghs, G., Michielsen, M., et al. 2018, ApJS, 237, 15
Aerts, C., Mathis, S., & Rogers, T. M. 2019, ARA&A, 57, 35
Aerts, C., Augustson, K., Mathis, S., et al. 2021, A&A, 656, A121
Antoci, V., Cunha, M. S., Bowman, D. M., et al. 2019, MNRAS, 490, 4040
Bailer-Jones, C. A. L., Rybizki, J., Fouesneau, M., Mantelet, G., & Andrae, R. 2018, AJ, 156, 58
Balona, L. A. 1986, MNRAS, 219, 111
Balona, L. A., & Ozuyar, D. 2020, MNRAS, 493, 5871
Baluev, R. V. 2008, MNRAS, 385, 1279
Borucki, W. J., Koch, D., Basri, G., et al. 2010, Science, 327, 977
Bowman, D. M., Aerts, C., Johnston, C., et al. 2019, A&A, 621, A135
Bowman, D. M., Burssens, S., Simón-Díaz, S., et al. 2020, A&A, 640, A36
Briquet, M., & Aerts, C. 2003, A&A, 398, 687
Briquet, M., Aerts, C., Mathias, P., Scuflaire, R., & Noels, A. 2003, A&A, 401, 281
Burssens, S., Simón-Díaz, S., Bowman, D. M., et al. 2020, A&A, 639, A81
Claveria, R. M., Mendez, R. A., Silva, J. F., & Orchard, M. E. 2019, PASP, 131, 084502
Clementini, G., Ripepi, V., Garofalo, A., et al. 2023, A&A, in press, https://doi.org/10.1051/0004-6361/202243964
Creevey, O. L., Sordo, R., Pailler, F., et al. 2023, A&A, in press, https://doi.org/10.1051/0004-6361/202243688
Cuypers, J., Aerts, C., De Cat, P., et al. 2009, A&A, 499, 967
Daszyńska-Daszkiewicz, J., Pamyatnykh, A. A., Walczak, P., et al. 2017, MNRAS, 466, 2284
De Cat, P., & Aerts, C. 2002, A&A, 393, 965
De Cat, P., Aerts, C., De Ridder, J., et al. 2000, A&A, 355, 1015
De Cat, P., Briquet, M., Daszyńska-Daszkiewicz, J., et al. 2005, A&A, 432, 1013
De Cat, P., Eyer, L., Cuypers, J., et al. 2006, A&A, 449, 281
De Cat, P., Briquet, M., Aerts, C., et al. 2007, A&A, 463, 243
De Pauw, M., Aerts, C., & Waelkens, C. 1993, A&A, 280, 493
De Ridder, J., Molenberghs, G., Eyer, L., & Aerts, C. 2016, A&A, 595, A3
Dupret, M. A., Grigahcène, A., Garrido, R., Gabriel, M., & Scuflaire, R. 2005, A&A, 435, 927
Edelmann, P. V. F., Ratnasingam, R. P., Pedersen, M. G., et al. 2019, ApJ, 876, 4
Eyer, L., & Mowlavi, N. 2008, J. Phys. Conf. Ser., 118, 012010
Eyer, L., Audard, M., Holl, B., et al. 2023, A&A, in press, https://doi.org/10.1051/0004-6361/202244242
Frémat, Y., Royer, F., Marchal, O., et al. 2023, A&A, in press, https://doi.org/10.1051/0004-6361/202243809
Gaia Collaboration (Brown, A. G. A., et al.) 2016a, A&A, 595, A2
Gaia Collaboration (Prusti, T., et al.) 2016b, A&A, 595, A1
Gaia Collaboration (Eyer, L., et al.) 2019, A&A, 623, A110
Gaia Collaboration (Brown, A. G. A., et al.) 2021, A&A, 649, A1
Gaia Collaboration (De Ridder, J., et al.) 2023a, A&A, in press, https://doi.org/10.1051/0004-6361/202243767 (Paper I)
Gaia Collaboration (Vallenari, A., et al.), et al. 2023b, A&A, in press, https://doi.org/10.1051/0004-6361/202243940
Gebruers, S., Straumit, I., Tkachenko, A., et al. 2021, A&A, 650, A151
Gilliland, R. L., Brown, T. M., Christensen-Dalsgaard, J., et al. 2010, PASP, 122, 131
Grassitelli, L., Fossati, L., Langer, N., et al. 2015a, A&A, 584, A2
Grassitelli, L., Fossati, L., Simón-Diáz, S., et al. 2015b, ApJ, 808, L31
Guzik, J. A., Kaye, A. B., Bradley, P. A., Cox, A. N., & Neuforge, C. 2000, ApJ, 542, L57
Handler, G. 1999, MNRAS, 309, L19
Holl, B., Audard, M., Nienartowicz, K., Jevardat de Fombelle, G., & Marchal, O. 2018, A&A, 618, A30
Horst, L., Edelmann, P. V. F., Andrássy, R., et al. 2020, A&A, 641, A18
Katz, D., Sartoretti, P., Guerrier, A., et al. 2023, A&A, in press, https://doi.org/10.1051/0004-6361/202244220
Kaye, A. B., Handler, G., Krisciunas, K., Poretti, E., & Zerbi, F. M. 1999, PASP, 111, 840
Keen, M. A., Bedding, T. R., Murphy, S. J., et al. 2015, MNRAS, 454, 1792
Kurtz, D. W., Saio, H., Takata, M., et al. 2014, MNRAS, 444, 102
Lebzelter, T., Mowlavi, N., Lecoeur-Taibi, I., et al. 2023, A&A, in press, https://doi.org/10.1051/0004-6361/202244241
Li, G., Bedding, T. R., Murphy, S. J., et al. 2019, MNRAS, 482, 1757
Li, G., Van Reeth, T., Bedding, T. R., et al. 2020, MNRAS, 491, 3586
Marton, G., Ábrahám, P., Rimoldini, L., et al. 2023, A&A, in press, https://doi.org/10.1051/0004-6361/202244101
Mathias, P., Aerts, C., De Pauw, M., Gillet, D., & Waelkens, C. 1994, A&A, 283, 813
Mathias, P., Aerts, C., Briquet, M., et al. 2001, A&A, 379, 905
Mathias, P., Le Contel, J. M., Chapellier, E., et al. 2004, A&A, 417, 189
Molenberghs, G., & Kenward, M. 2007, Missing Data in Clinical Studies (New York: John Wiley)
Mombarg, J. S. G., Van Reeth, T., Pedersen, M. G., et al. 2019, MNRAS, 485, 3248
Mombarg, J. S. G., Van Reeth, T., & Aerts, C. 2021, A&A, 650, A58
Moravveji, E. 2016, MNRAS, 455, L67
Moravveji, E., Townsend, R. H. D., Aerts, C., & Mathis, S. 2016, ApJ, 823, 130
Murphy, S. J., Fossati, L., Bedding, T. R., et al. 2016, MNRAS, 459, 1201
Pápics, P. I., Tkachenko, A., Van Reeth, T., et al. 2017, A&A, 598, A74
Pedersen, M. G. 2022a, ApJ, 930, 94
Pedersen, M. G. 2022b, ApJ, 940, 49
Pedersen, M. G., Chowdhury, S., Johnston, C., et al. 2019, ApJ, 872, L9
Pedersen, M. G., Aerts, C., Pápics, P. I., et al. 2021, Nat. Astron., 5, 715
Raskin, G., van Winckel, H., Hensberge, H., et al. 2011, A&A, 526, A69
Rimoldini, L., Holl, B., Gavras, P., et al. 2023, A&A, in press, https://doi.org/10.1051/0004-6361/202245591
Ripepi, V., Clementini, G., Molinaro, R., et al. 2023, A&A, in press, https://doi.org/10.1051/0004-6361/202243990
Rogers, T. M., Lin, D. N. C., McElwaine, J. N., & Lau, H. H. B. 2013, ApJ, 772, 21
Saio, H., Kurtz, D. W., Takata, M., et al. 2015, MNRAS, 447, 3264
Saio, H., Kurtz, D. W., Murphy, S. J., Antoci, V. L., & Lee, U. 2018, MNRAS, 474, 2774
Salpeter, E. E. 1955, ApJ, 121, 161
Sartoretti, P., Blomme, R., David, M., & Seabroke, G. 2022, Gaia DR3 Documentation Chapter 6: Spectroscopy, European Space Agency; *Gaia* Data Processing and Analysis Consortium
SAS Institute Inc. 2014, SAS OnlineDoc 9.4 (Cary, NC: SAS Institute Inc.)
Sekaran, S., Tkachenko, A., Johnston, C., & Aerts, C. 2021, A&A, 648, A91
Serebriakova, N., Tkachenko, A., Gebruers, S., et al. 2023, A&A, submitted
Simón-Díaz, S., & Herrero, A. 2014, A&A, 562, A135
Simón-Díaz, S., Herrero, A., Uytterhoeven, K., et al. 2010, ApJ, 720, L174
Simón-Díaz, S., Godart, M., Castro, N., et al. 2017, A&A, 597, A22
Szewczuk, W., & Daszyńska-Daszkiewicz, J. 2017, MNRAS, 469, 13
Tkachenko, A., Aerts, C., Yakushechkin, A., et al. 2013, A&A, 556, A52
Tkachenko, A., Pavlovski, K., Johnston, C., et al. 2020, A&A, 637, A60
Triana, S. A., Moravveji, E., Pápics, P. I., et al. 2015, ApJ, 810, 16
Uytterhoeven, K., Moya, A., Grigahcène, A., et al. 2011, A&A, 534, A125
Van Reeth, T., Tkachenko, A., Aerts, C., et al. 2015, ApJS, 218, 27
Van Reeth, T., Tkachenko, A., & Aerts, C. 2016, A&A, 593, A120
Van Reeth, T., Mombarg, J. S. G., Mathis, S., et al. 2018, A&A, 618, A24
Waelkens, C. 1991, A&A, 246, 453
Waelkens, C., Aerts, C., Kestens, E., Grenon, M., & Eyer, L. 1998, A&A, 330, 215
Xiong, D. R., Deng, L., Zhang, C., & Wang, K. 2016, MNRAS, 457, 3163
Zwintz, K., Van Reeth, T., Tkachenko, A., et al. 2017, A&A, 608, A103

Appendix A: Plots of the predictors for vsini_esphs

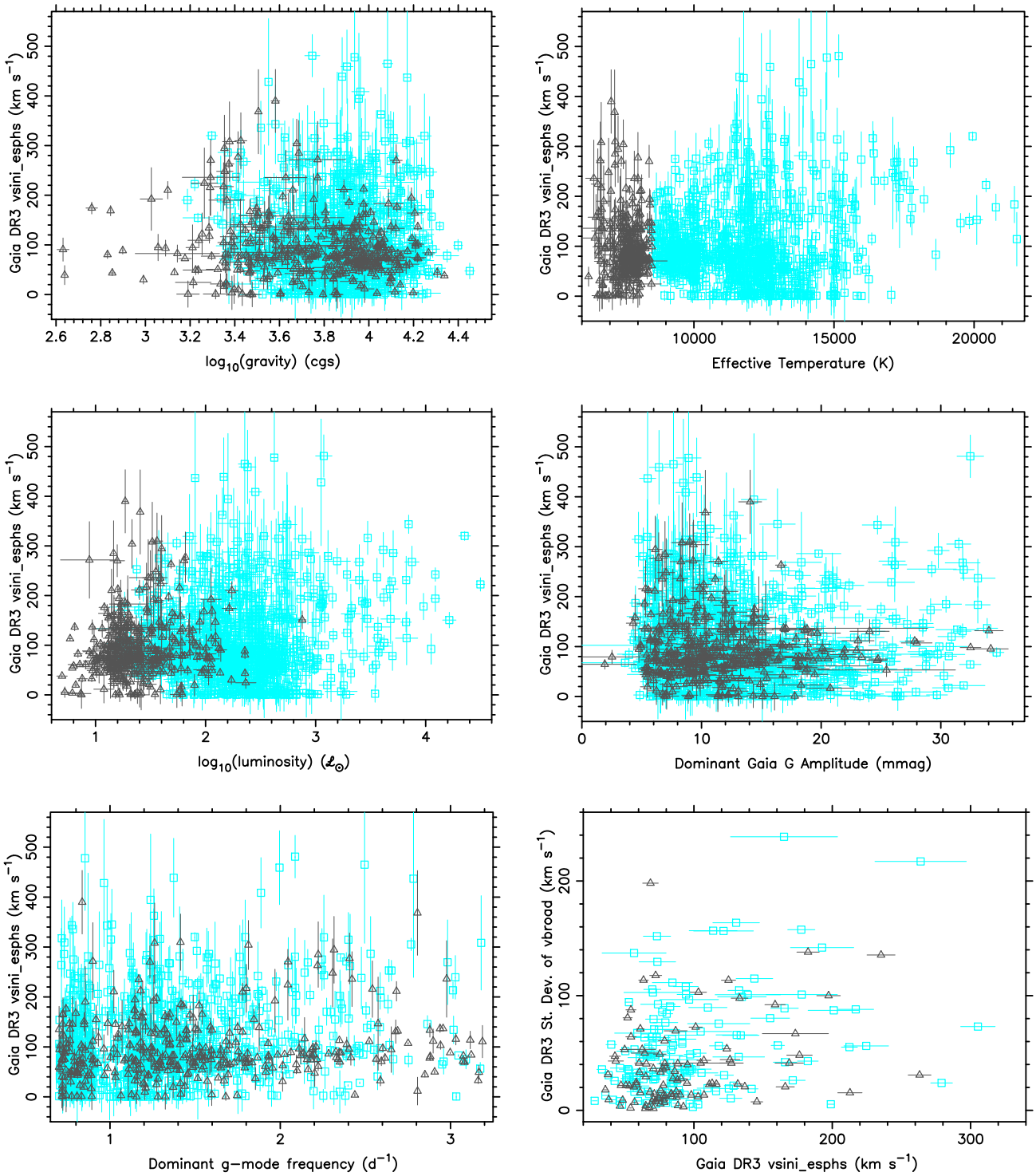

Fig. A.1. Gaia DR3 measurements of vsini_esphs versus each of the five covariates as indicated for the 384 γ Dor (grey triangles) and 1104 SPB (cyan squares) stars for which these quantities are available. The lower right panel shows the standard deviation of vbroad as a function of vsini_esphs for the 100 γ Dor and 190 SPB stars for which these quantities are available. When invisible, the errors are smaller than the symbol sizes.

Appendix B: Regression models for the standard deviation of `vbroad`

The quantity `vbroad` can be considered a simplified estimate of the time-dependent second moment of a line profile (Aerts et al. 1992; De Pauw et al. 1993; Mathias et al. 1994; Briquet & Aerts 2003). It is therefore meaningful to investigate whether or not the standard deviation of `vbroad` contains information on the time-dependent line-profile variability of the Gaia DR3 g-mode pulsators.

In order to compute backward-selection regression models for this quantity, we now add `vsini_esphs` as a sixth covariate (with β_6 as notation for its regression coefficient). In line with Simón-Díaz & Herrero (2014) and Aerts et al. (2014b), Serebriakova et al. (2023) found from simulations that the projected rotational velocity should first be derived from high-resolution spectra before any meaningful derivation of left-over additional time-dependent spectral-line broading caused by tangential velocity fields can be done. This is in agreement with the methodology used by Aerts et al. (2014b) to assess the quality of estimates for time-dependent macroturbulent broadening from the line's moment variations in well-known B-type pulsators.

Table B.1. Estimates (standard errors) for the parameters of the errors-in-variables model for the standard deviation of `vbroad` measured for the 1775 Gaia DR3 γ Dor stars. The results are based on backward selection considering a set of six (top) or five (bottom) predictors.

Effect	Par.	Estimate (s.e.)	p-value	95% conf. int.
With `vsini_esphs` — $R^2 = 0.09$				
Intercept	β_0	−459(146)		[−750;−169]
log g	β_2	93(29)	0.0019	[35;151]
$\log(L/\mathcal{L}_\odot)$	β_3	85(27)	0.0019	[32;138]
`vsini_esphs`	β_6	0.26(0.08)	0.0018	[0.10;0.42]
Res. var.	σ^2	1122(166)	<0.0001	[793;1452]
Without `vsini_esphs` — $R^2 = 0.06$				
Intercept	β_0	−517(135)		[−781;−253]
log $T_{\rm eff}$	β_1	136(35)	0.0001	[66;205]
$\log(L/\mathcal{L}_\odot)$	β_3	11(3)	<0.0001	[6;16]
ν	β_4	8(1)	<0.0001	[6;10]
A_ν	β_5	−200(88)	0.0234	[−374;−27]
Res. var.	σ^2	497(17)	<0.0001	[464;529]

Table B.1 displays the regression models for the standard deviation of `vbroad` for the sample of 1775 Gaia DR3 γ Dor stars. We perform the backward selection twice: once with the covariate `vsini_esphs` and once without it. For the model including it as a potential predictor, we remove the insignificant contributions of the variables log g, A_ν, and $\log(L/\mathcal{L}_\odot)$ (in that order). Not suprisingly, `vsini_esphs` is a significant predictor for the standard deviation of `vbroad`, along with the gravity and luminosity of the star. For the regression model without `vsini_esphs`, only log g is removed and the predictive power decreases from 9% to 6% of the original variance.

The combined results in Tables 3, 4, and B.1 reveal that rotational broadening of γ Dor stars dominates the measurement of `vbroad`, while the evolutionary status (by means of the gravity and/or effective temperature) lies at the basis of the significant predictors of `vbroad`. Regression models for the standard deviation have low predictive power and are thus harder to interpret, in line with the caveats due to the systematic uncertainties connected with the treatments of microturbulent broadening, log g, and $T_{\rm eff}$ highlighted by Tkachenko et al. (2020).

Table B.2. Estimates (standard errors) for the parameters of the errors-in-variables model for the standard deviation of `vbroad` measured for the 190 Gaia DR3 SPB pulsators. The results are based on backward selection considering a set of six (top) or five (bottom) predictors.

Effect	Par.	Estimate (s.e.)	p-value	95% conf. int.
With `vsini_esphs` — $R^2 = 0.20$				
Intercept	β_0	−515(246)		[−1001;−30]
log $T_{\rm eff}$	β_1	138(61)	0.0256	[17;258]
ν	β_4	−17(6)	0.0031	[−28;−6]
`vsini_esphs`	β_6	0.39(0.06)	<0.0001	[0.26;0.52]
Res. var.	σ^2	1324(156)	<0.0001	[1016;1631]
Without `vsini_esphs` — $R^2 = 0.01$				
Intercept	β_0	−515(237)		[−382;−48]
log $T_{\rm eff}$	β_1	140(59)	0.0185	[24;256]
Res. var.	σ^2	1641(169)	<0.0001	[1308;1974]

As for the SPB pulsators, Table B.2 displays the regression models for the standard deviation of `vbroad` from backward selection for the 190 SPB stars with such measurements. For the model with the covariate `vsini_esphs` included as a potential predictor, the order of variables to be removed was log g, A_ν, and $\log(L/\mathcal{L}_\odot)$. The model explains 20% of the variance in the standard deviation of `vbroad` and has `vsini_esphs`, log $T_{\rm eff}$, and ν as significant predictors. For the model without `vsini_esphs` as a potential predictor, all covariates aside from log $T_{\rm eff}$ were removed as insignificant and the predictive power disappears. Therefore, we find that the standard deviation of the `vbroad` measurements of SPB stars is affected by their surface rotation and is connected to their effective temperature and dominant g-mode frequency.

The regression models for the standard deviation of `vbroad` have low (SPB stars) to almost no (γ Dor stars) predictive power. This is not surprising, as this standard deviation is, at best, just one single value capturing the complicated overall time-dependent broadening determined from only a few scans across Gaia's field of view. Our findings suggest that the noise contribution to the standard deviation of `vbroad` dominates over the one due to the astrophysical parameters for the γ Dor stars.